

JRC TECHNICAL REPORTS

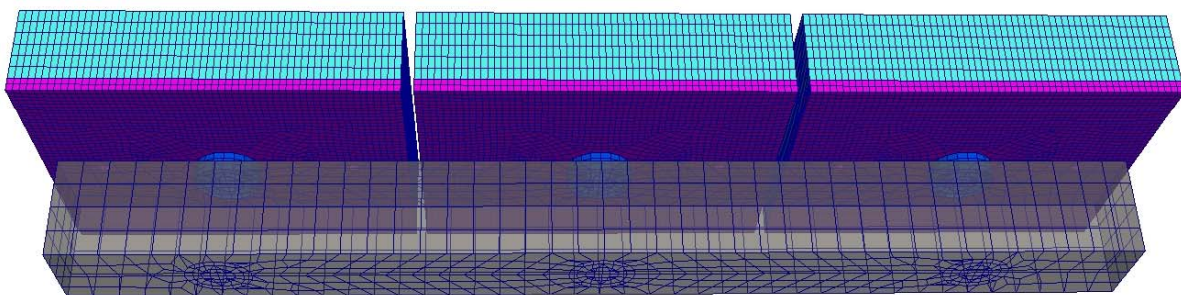
Numerical simulation in support of the blast actuator development part II

Georgios Valsamos

Martin Larcher

George Solomos

2015



Numerical simulation in support of the blast actuator development part II

This publication is a Technical report by the Joint Research Centre, the European Commission's in-house science service. It aims to provide evidence-based scientific support to the European policy-making process. The scientific output expressed does not imply a policy position of the European Commission. Neither the European Commission nor any person acting on behalf of the Commission is responsible for the use which might be made of this publication.

JRC Science Hub

<https://ec.europa.eu/jrc>

JRC94812

EUR 27560 EN

ISBN 978-92-79-53473-7 (pdf)

ISSN 1831-9424 (online)

doi:10.2788/22569 (online)

© European Union, 2015

Reproduction is authorised provided the source is acknowledged.

Printed in Italy

All images © European Union 2015

How to cite: Authors; title; EUR; doi

Table of contents

Abstract.....	2
1 Introduction.....	3
2 Numerical model	4
2.1 Experimental facility.....	4
2.2 Finite element model	6
3 Hyperelastic material	12
3.1 Foam impact	12
3.2 New material model for sponge foams.....	21
3.2.1 Ogden-Storåkers hyperelastic foam	21
3.2.2 Examples.....	23
4 Numerical results.....	25
4.1 Blast 15.....	25
4.2 Blast 16.....	33
5 Conclusions	42
6 References	44
7 Appendix.....	45
7.1 Blast	45

Abstract

The development of the blast actuator experimental device is now entering the second phase, where reinforced concrete beams are used as specimens. This demanding phase needs a lot of support from numerical simulation to both predict and resolve possible failures and to validate the test results. The current report presents the comparison between the experimental and numerical results, focusing on the justification of the appearing discrepancies. Moreover, interesting information, that can ameliorate the final configuration of the apparatus, is extracted after the interpretation of the numerical results.

1 Introduction

This report is a sequel to reports [1], [9] on the numerical simulation support of the blast actuator experimental device. The blast actuator project [2], which targets to simulate explosive events on structural components (e.g. reinforced concrete columns) without using real explosives, is moving to the second face. After the calibration of some critical parameters of the apparatus, the first tests on real reinforced concrete columns are taking place. The objective of the current study is to verify the results of the first set of experiments with numerical calculations and to provide some information that can ameliorate the final configuration of the apparatus.

The report is divided into three chapters. The first one presents the current set up of the experimental device. The dimensions and the material properties of the column specimen are shown. The equivalent finite element model that is used for the numerical calculations is presented. Details like the material properties, the boundary conditions and the impact-contact model are discussed.

The next chapter presents developments that took place in order to optimize the material law used to simulate the elastic foam material in numerical simulations. An elastic foam layer is located in the contact interface of the specimen and the impacting mass in order to make the impact smoother. The mechanical behaviour of the elastic foam is represented in a more realistic way through the [16] formulation.

The fourth chapter presents the numerical results of the simulation. The numerical simulations are performed with EUROPLEXUS finite element code [4]. EUROPLEXUS is an explicit finite element computer code for fast transient dynamic analysis of fluid-structure systems jointly developed by the Joint Research Centre (JRC Ispra) and the French Commissariat à l'Énergie Atomique et aux Énergies Alternatives (CEA Saclay). A comparison of the numerical and the experimental results is taking place. The differences are justified and some solutions are proposed in order to optimize the experimental apparatus.

The last chapter concludes the report and highlights the results from the numerical investigation. All input files used for the numerical calculations are included in the appendix.

2 Numerical model

The blast simulator facility concept is based on a fast actuator that accelerates a mass which afterwards impacts on the specimen in such a way that the produced force is similar to the one from a real explosive event. This is a way to perform experimental tests on critical structural components in a safer and more controllable way than using real explosive materials.



Figure 1: The blast actuator apparatus in ELSA

2.1 Experimental facility

The ELSA blast simulator in Figure 1 is a complicated device, which can be separated into two main parts, as can be observed in Figure 2. The first part consists of the hydraulic actuator, the nitrogen charging device, the piston, the shaft and the fragile bolt. The hydraulic actuator compresses the spring to the starting position. The piston is kept in the initial position by a fragile bolt (high strength steel). A nitrogen charging device puts pressure on the fragile bolt which after a certain limit breaks and releases the piston and the shaft of the blast actuator and accelerates the impacting mass. This part of the blast actuator is not considered in the numerical simulations.

The second part of the device is the impacting mass that is accelerated from the actuator and hits the specimen in order to cause a blast loading on it. The impacting mass is considered in the simulation, but its modelization is simple in the sense that some of the structural details (bolts etc.) of the design are neglected. The impacting mass is accelerated by the fast actuator and strikes the specimen, which is supported on the reaction wall.

The impacting mass consists of a massive metallic part, three aluminium plates, three load cells and three layers of elastic foam. The massive steel parallelepiped object represents the main part of the weight of the impacting mass. The representation of the details on that object is not important for the numerical simulation therefore it is modelled without many details. The aluminium plates will transfer the force from the accelerated mass on the specimen through the elastic foam layers. The load cells are mounted between the steel object and the aluminium plates in order to measure the transferred load. Two additional load cells are located on the supporting configuration of the specimen (between the specimen and the reaction wall) in order to measure the reaction force (Figure 4).

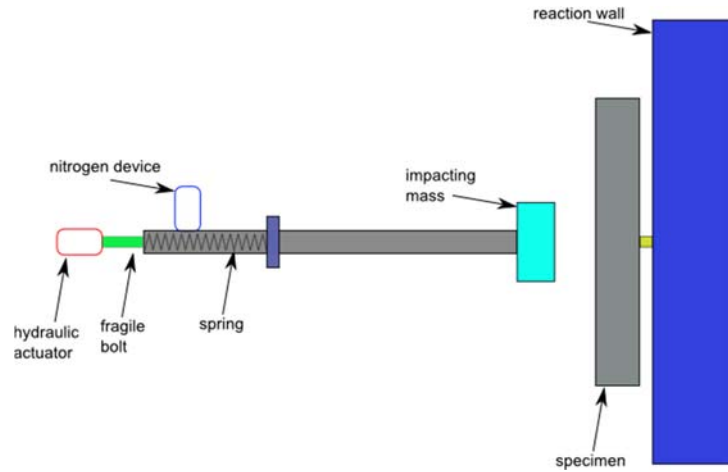


Figure 2: Sketch of the blast actuator

Figure 3 presents the set-up and the dimensions of the impacting mass that will be modelled for the numerical simulation. Figure 4 shows the top view of the experimental device just before the impact with the specimen. The parts of the impacting mass are marked with colours similar to the ones used for the sketch.

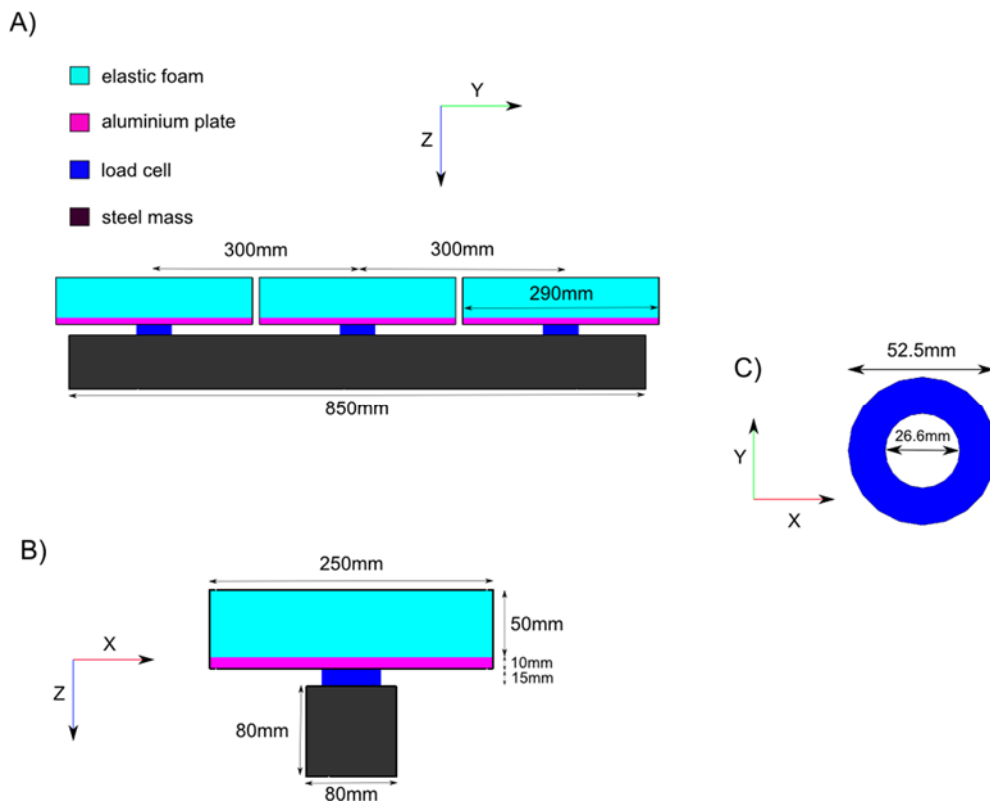


Figure 3: Sketch of the impacting mass

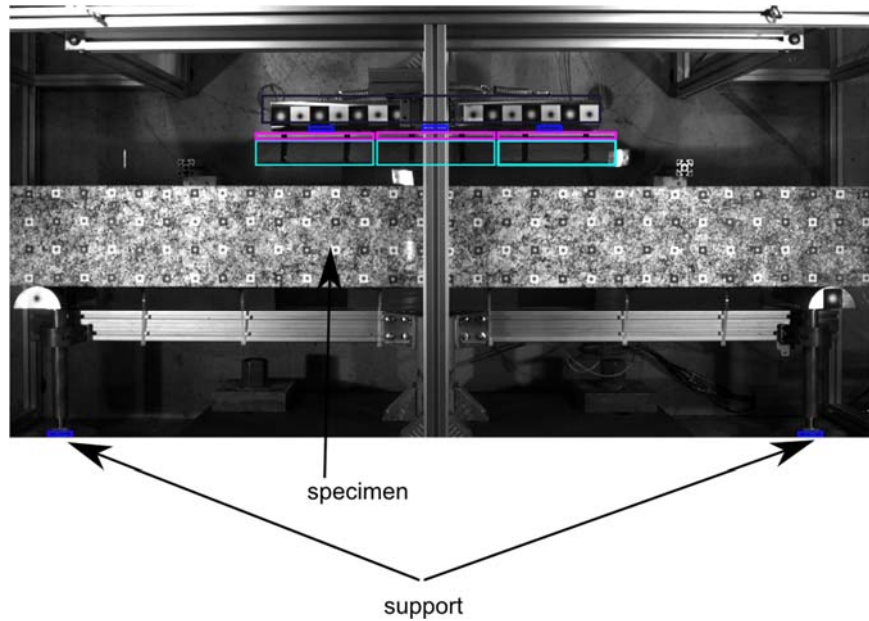


Figure 4: Top view of the impacting mass before it crash onto the specimen

2.2 Finite element model

The geometrical model presented in Figure 3 has been discretized with finite elements by using the CAST3M code [5]. The geometry is simple enough so the main concern in the modelling is how fine should be the mesh. Four different parts are employed in the representation of the impacting mass. In the steel massive part a relatively coarse mesh has been used since is an object that will not undergo high strains so in that case bigger finite elements (average cubic edge size equal to 20mm) will results into a smaller model without sacrificing the accuracy of the outputs.

On the other hand for the load cells, the aluminium plates and the elastic foam layers finer mesh has been used. The average cubic edge size in that case is 5mm. The thickness of the aluminium plate is 10mm so it is prudent to have at least two layers of finite elements in this direction for an accurate representation of the bending behaviour. The thickness of the elastic foam layer is 50mm so in the first calculations ten layers of finite elements has been used in that direction. This resulted into a huge number of elements in the numerical model and high computational time. In the second step of the numerical calculations, a model with five layers of finite elements was tested (10mm edge size through the thickness) and it came out that although the size of the model and computational time were decreased the accuracy on the results was the same.

Table 1: Data concerning the mesh of the elastic foam layer

Number of layers	Element thickness [mm]	Number of elements	CPU time [s]
5	10mm	49464	100070
10	5mm	98928	150562

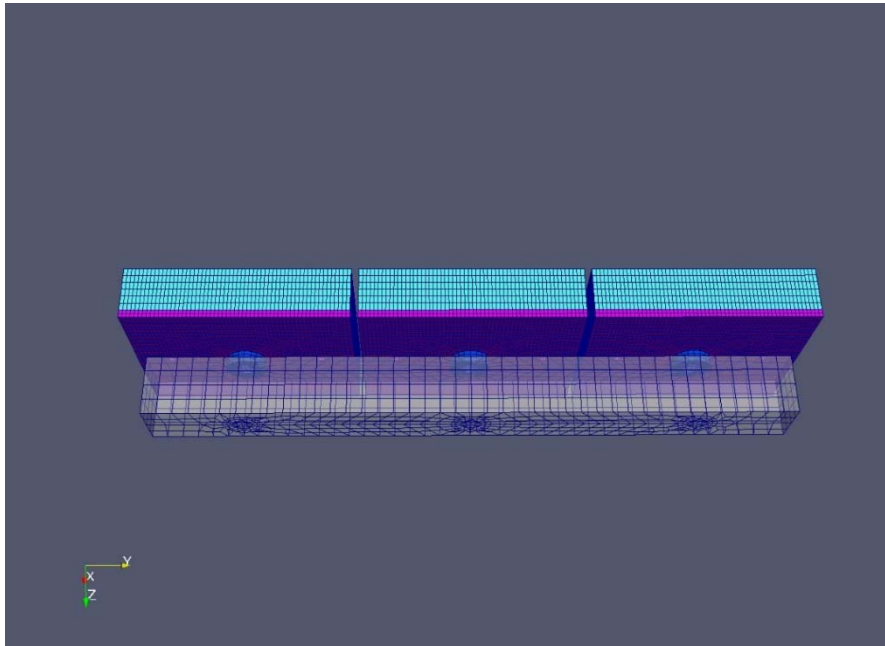


Figure 5: Finite element model of the impacting mass

Figure 5 presents the finite element model of the impacting mass of the blast actuator apparatus. For the steel part of the model and the load cells, the "VM23" material law of EUROPLEXUS has been used. The constructor provided the stiffness for each load cell ($K=14kN/m$). The volume and the mass of each load cell was easy to calculate so the desired density input computed via a simple division ($D=M/V$, D is the density, M the mass and V the volume). The poisson ratio is taken 0.3 since it is a mainly consisted by steel.

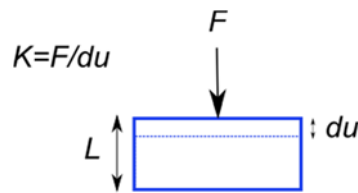


Figure 6: Compression of the load cell in terms of force and deformation

In order to calculate the Young's modulus from the stiffness the following process has been followed. The stiffness expresses the force F needed to compress the load cell for du as shown in Figure 6. The force can be re-written as $F = \sigma A$, where σ, A are the stress and the applied area respectively. The stress can also be written as $\sigma = \varepsilon E$, the product of strain (ε) and Young's modulus (E). With the association of the thickness L of the load cell and with the assumption that $\varepsilon = du/L$ the final formulation of the Young's modulus for the load cell is produced as shown in the next set of equations:

$$\begin{aligned}
 K &= \frac{F}{du} = \frac{\sigma A}{du} = \frac{(\varepsilon E) A L}{du L} \Leftrightarrow \\
 K &= \frac{EA \varepsilon L}{L du} = \frac{EA}{L} \Leftrightarrow \\
 E &= \frac{KL}{A}
 \end{aligned}
 \tag{1}$$

Equation (1) expresses the Young's modulus of the load cell in relation with known quantities like the stiffness K the thickness L and the area of the connecting surface.

The plates of the impacting mass that will transfer the load to the specimen are made of aluminium, since it is a material with high strength/weight ratio. This mechanical characteristic of

aluminium is very important for the present experimental device, since the impacting mass can have high strength and relatively light plates in the front part of the configuration. Substituting the aluminium plates with steel ones, it will cause an increase in the total mass of about 25%. Aluminium material after reaching the elastic limit is behaving as nearly plastic so the “VMIS PARF” material law has been used in EUROPLEXUS. Table 2 presents all the material properties for the metallic parts of the impacting mass.

For the elastic foam layers the input from the laboratory was the stress-strain curve Figure 7. The “HYPE” type 5 material law of EUROPLEXUS has been used since it is giving as it shows the next chapter the most realistic results. After a best-fit procedure [9] of the given stress-strain curve, the input parameters for the strain energy equation of the hyperelastic material have been defined Table 3.

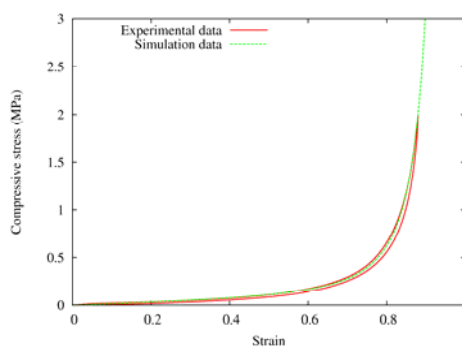


Figure 7: Stress-strain curve for the elastic foam material

Table 2: Material data for the metallic part of the impacting mass

Part	Density [kg/m ³]	Young's modulus [N/m ²]	Poisson ratio	Elastic limit [MPa]
Steel block	7500	2.1e1	0.3	400
Aluminium plate	2800	70e9	0.35	400
Load cell	6488	1.31e11	0.3	400

Table 3: Material data for the elastic foam material (type 5)

Density [kg/m ³]	C01	C02	C05	C06	C09	C10
42	72.86	72.29	20123	90.71	0.0168	0.0649

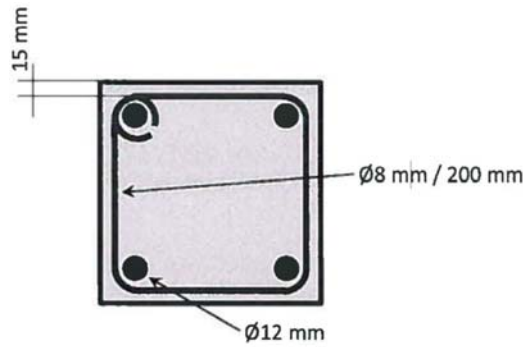


Figure 8: Data for the reinforcement of the specimen column

The specimen for the experiment is reinforced concrete column and its characteristics are presented in Table 4, Figure 8. The column is located horizontally to the floor placed on two brackets (almost 20cm above the floor). The rear face of the column is vertically supported on the reaction wall on two points with a span of 2m as shown in Figure 9. The concrete column has been discretized with cubic finite elements with edge size 20mm. This size of elements is sufficient for that step of simulation since the objective is to calculate the impacting force of the mass on the specimen. In later experiments where the failure of the column will be the dominant phenomenon finer mesh for the discretization of the column will be used. The reinforcement of the column has been modelled with bar (BR3D) elements.

Table 4: Data of the reinforced concrete column specimen

Width [m]	Depth [m]	Height [mm]	Longitudinal reinforcement [mm]	Hoop [mm]
250	250	2200	4D12	10D8

The bonding between the concrete and the reinforcement has been modelled via the "ARMAT" directive of EUROPLEXUS [3]. This directive allows to link the displacements of the nodes belonging to continuum-like elements made of concrete, with those of bar-like elements made of steel. For the simulation of the support of the column, the finite element mesh has been blocked in the vertical direction for all the points lying on the support lines as shows Figure 9.

The pinball method [7], [8] has been used for the contact between the impacting mass and the specimen. The implementation is similar to the one described in the previous report [1]. There are two contact bodies, the impacting mass and the column specimen. From the impacting mass only the foam layer is participating in the contact body while from the column the part the surface slightly wider than the projection of the impactor onto the specimen Figure 10.

There are no many information available for the material properties of the reinforced concrete column. The constructor of the specimens has define the unconfined compressive strength and the maximum aggregate size. A typical value has been used for the Young's modulus and the Poisson ration. It is planned to test some cubic specimen of the concrete column in the laboratory so in the future more accurate data concerning the strain rate effect will be available. The "DPDC" material load (vers=8) has been used for the simulation of the concrete material in EUROPLEXUS [3]. The "DPDC" material law is a three-invariant cap model with mixed hardening and isotropic damage that contains also the strain-rate effect [17]. The basic input for this directive are the Young's modulus, the Poisson's ratio, the unconfined compression test and the maximum aggregate size all the other parameters are computed internally in the subroutine of the code. For

the steel reinforcement the “VMIS ISOT” material has been used. The material properties for the RC column are presented in Table 5, Table 6 respectively.

Table 5: Concrete material properties

Density [kg/m ³]	Young's modulus [N/m ²]	Poisson ratio	Unconfined compressive strength [N/m ²]	Maximum aggregate size [mm]
2400	30e9	0.21	20e6	20

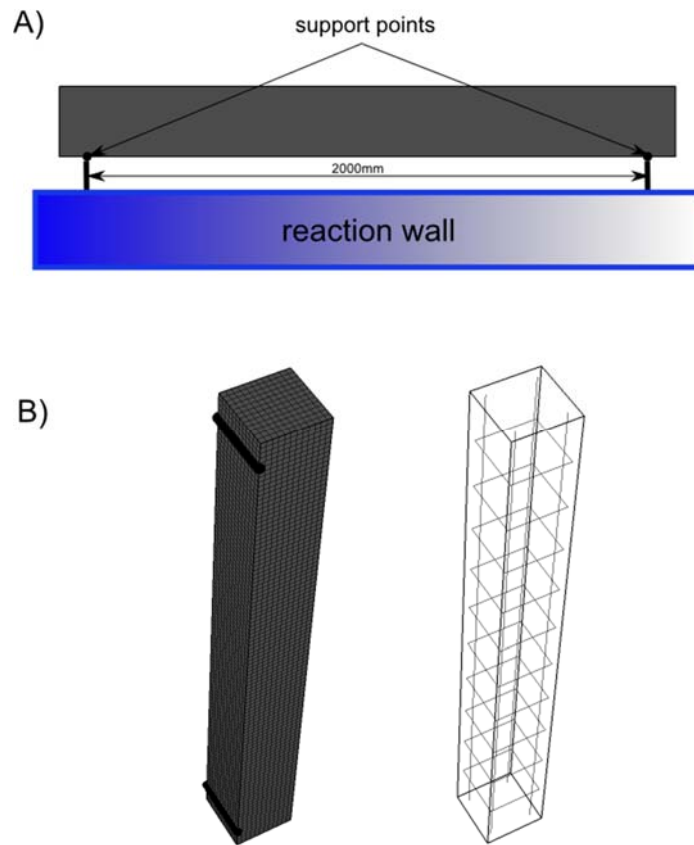


Figure 9: Support points and finite element mesh of the RC column specimen

Table 6: Steel properties (for the reinforcement)

Density [kg/m ³]	Young's modulus [N/m ²]	Poisson ratio	Yield stress [N/m ²]	Ultimate strength [mm]	Fracture strain
---------------------------------	--	---------------	-------------------------------------	---------------------------	-----------------

7800	20e11	0.3	850e6	1035e6	0.12
------	-------	-----	-------	--------	------

Table 7 presents the mass of each part of the impacting mass and their percentage of the total mass. It is clear that the major part of the mass is located in the steel block (86%) as expected. The total mass of the aluminium plates is almost 6 kg which is the 12% of the total mass. As already mentioned the aluminium has been selected because of its low density and it is much better than using steel plates. On the other hand, 12% of the mass is located on the plates and this might cause problems in the measuring of the force on the load cells since it can be behave as a filter of the contact force.

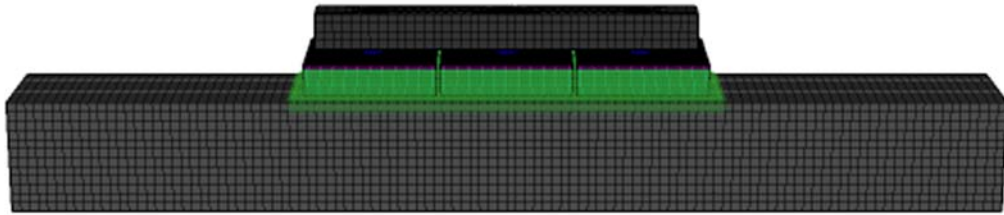


Figure 10: Pinballs of the contact bodies

Table 7: Mass data for the various parts of the impacting mass

Part	Mass [kg]	Ratio [%]
Steel block	40.49	86
Load cells	0.466	1
Aluminium plates	6.078	12
Elastic foam layers	0.548	1

3 Hyperelastic material

This chapter presents the developments that took place in Europlexus in order to optimize the behaviour of the foam interlayer between the specimen and the aluminium plates.

3.1 Foam impact

Peroni [2] has shown the possibilities that are given with the new blast actuator of the JRC. The first preliminary tests were done using metal tubes (some numerical investigations are shown in [1]) and cylindrical blocks built from plastic foam. Here, the experiments with the elastic foam are used in order to validate the numerical models. The foam used has a density of about 40 kg/m^3 . The foam blocks have had a radius of 9.25 cm and a thickness of 6 cm (Figure 11).

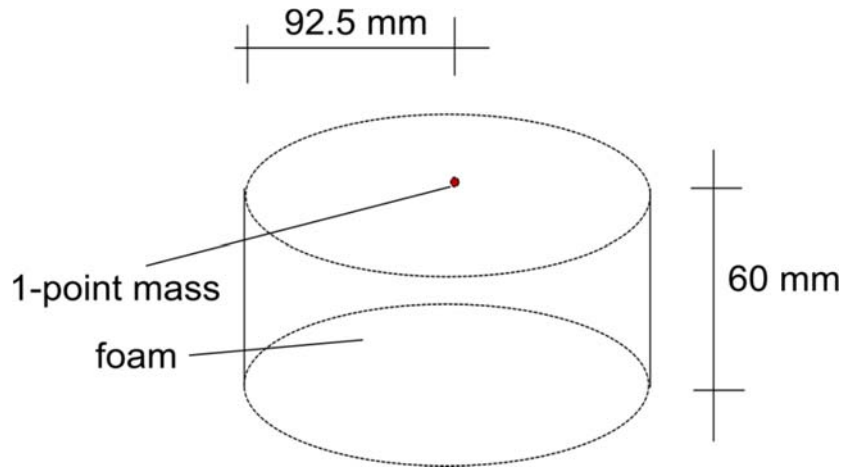


Figure 11: Geometry of the foam blocks

The models were built using LS-Prepost since that program offers a very easy way to create cylindrical meshes where the inner part is built from rectilinear hexahedrons and around of that inner part the hexahedrons are configured in order to get a circular outer surface (Figure 2). Two input parameters are needed; the number of elements in circumferential direction and the number of elements through the thickness.

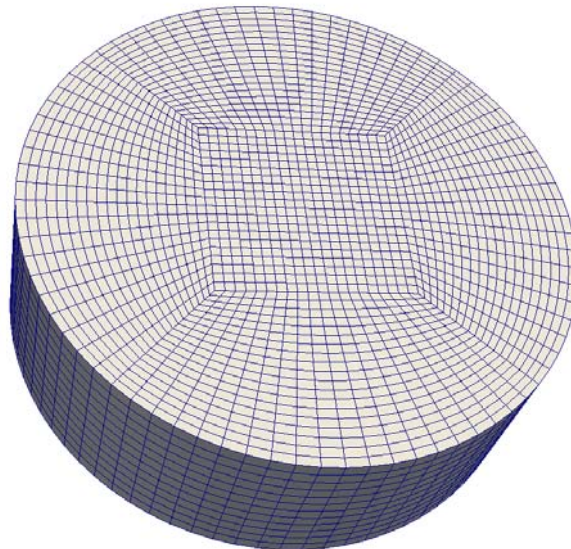


Figure 12: Geometry of the model foam_impact12

Two experiments were considered: experiment 10 with a speed of 8.7 m/s and experiment 11 with a speed of 5.1 m.

The nodes on the bottom of the model were set to fix in all directions. The nodes on the other side were fixed parallel to the area. The mass of the aluminium block of 40 kg is attached using a one-node element (PMAT) which node is independent from the foam mesh. The impact is introduced using the LINK IMPA method. This method allows defining one part with elements that impact another part in a given direction. In that way, the model can be created very efficient.

Two different material models were used: MAT_FOAM and MAT_HYPE. MAT_FOAM is a material law that is mainly developed for metal foam. The previous report [9] shows the adaptation of the material law to the elastic foam used here.

MAT_HYPE is a set of hyperelastic materials. Two types are investigated here: Mooney-Rivlin material (type 1) and Ogden material (type 4). For both types, the material parameters are calculated by using the PCAL command in EUROPLEXUS. Its objective is to get the material parameters by a best-fit approach of some measured stress-strain relations. This parameter identification should always be done newly with the recent version of the software since changes in the material routine can also affect these values.

The density of the numerical investigations was set to 134 kg/m³. This is slightly higher than the measured one.

Table 8 shows the investigated models Table 9 shows the input parameters for some particular cases.

Table 8: Parameter identification for a specific rubber: parameters

	Nb elem. Circumf er.	Nb elem. thickne ss	Speed	Material	Bulk modul us	Comments
foam_impact 2	20	4	8.7	VM23		Test model
foam_impact 3	40	8	8.7	MAT_HYPE 4	7e5	
foam_impact 4	40	8	8.7	MAT_HYPE 1		Shrinking
foam_impact 5	80	12	8.7	MAT_HYPE 4	7e5	
foam_impact 6	160	24	8.7	MAT_HYPE 4	7e5	
foam_impact 7	80	12	5.2	MAT_HYPE 4	7e5	

foam_impact 8	80	12	5.2	MAT_FOAM	-	No rebound
foam_impact 9	80	12	5.2	MAT_HYPE 4	7e5	
foam_impact 10	80	12	5.2	MAT_HYPE 4	7e6	Crazy
foam_impact 11	80	12	5.2	MAT_HYPE 4	7e4	End by NaN
foam_impact 12	80	12	5.2	MAT_HYPE 4	3e4	End by NaN
foam_impact 13	80	12	5.2	MAT_HYPE 4	7e5	Opt stress strain 0.94 5MPa
foam_impact 14	160	24	5.2	MAT_HYPE 4	7e5	
foam_impact 15	80	12	5.2	MAT_HYPE 4	7e5	0.90 5 MPa
foam_impact 16	40	6	5.2	MAT_HYPE 4	7e5	

Table 9: Input parameters for models foam_impact7-foam_impact12

Foam_impact7	Foam_impact9	Foam_impact11
HYPE TYPE 4 RO 134	HYPE TYPE 4 RO 134	HYPE TYPE 4 RO 134
BULK 7.44E+05	BULK 7.44E+05	BULK 74400.0000000000
CO1 -0.49239E-02	CO1 -0.13043E+00	CO1 -0.35025E+00
CO2 0.11001E+02	CO2 0.24410E+01	CO2 -0.49575E+00
CO3 0.11305E+02	CO3 0.56812E+01	CO3 0.25085E+01
CO5 0.50119E+06	CO5 0.19055E+06	CO5 0.19055E+06
CO6 0.43652E+04	CO6 0.39811E+05	CO6 0.66069E+06
CO7 0.10000E+05	CO7 0.54954E+04	CO7 0.22909E+06

Foam_impact8	Foam_impact10	Foam_impact12
MATE FOAM	HYPE TYPE 4 RO 134	HYPE TYPE 4 RO 134
RO_F 134	BULK 7440000.00000000	BULK 30000.0000000000
YOUN 375000	CO1 -0.13313E+00	CO1 0.33167E-01
NU 0.1	CO2 0.56812E+01	CO2 0.35748E+01
SIGP 15000	CO3 0.21890E+01	CO3 -0.52352E+00
RO_0 1050	CO5 0.54954E+06	CO5 0.19055E+06
ALFA 1.870829	CO6 0.54954E+04	CO6 0.10471E+06
GAMM 110000	CO7 0.75858E+05	CO7 0.60256E+06
ALF2 1000000		
BETA 6		

Figure 13 to Figure 22 shows the displacements after the experiment for several of the models. It must be concluded that the models cannot represent the material behaviour of the elastic foam very well. Figure 23 shows the displacement-history. It can be concluded that none of the models can represent the unloading of the sample. Especially the behaviour at the borders of the foam cylinder cannot be described very well with the classical Ogden materials. In some cases the discontinuity of the stress indicates additional problems in the material description.

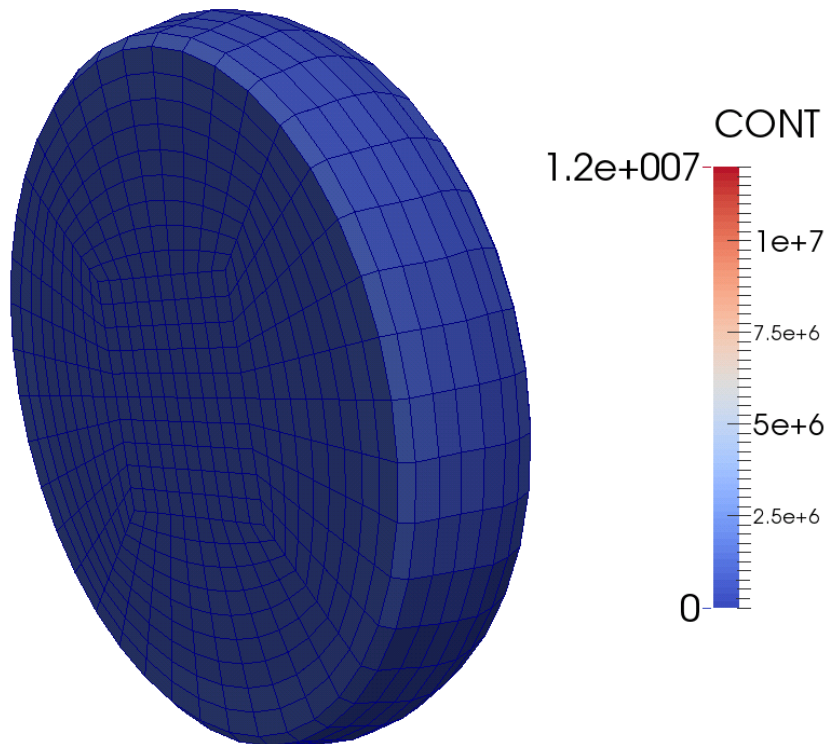


Figure 13: foam_impact3

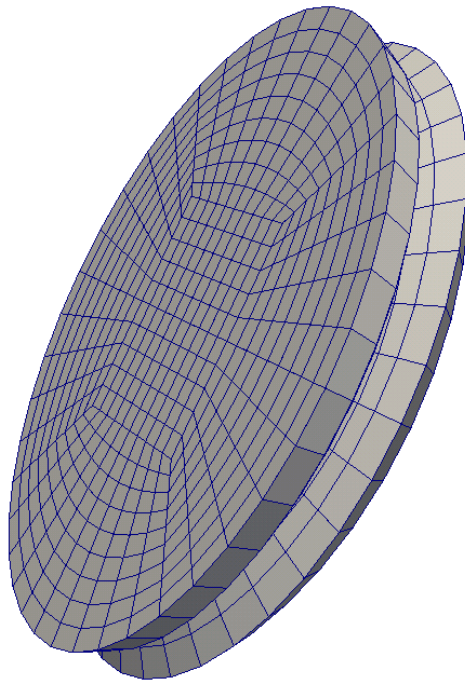


Figure 14: foam_impact4

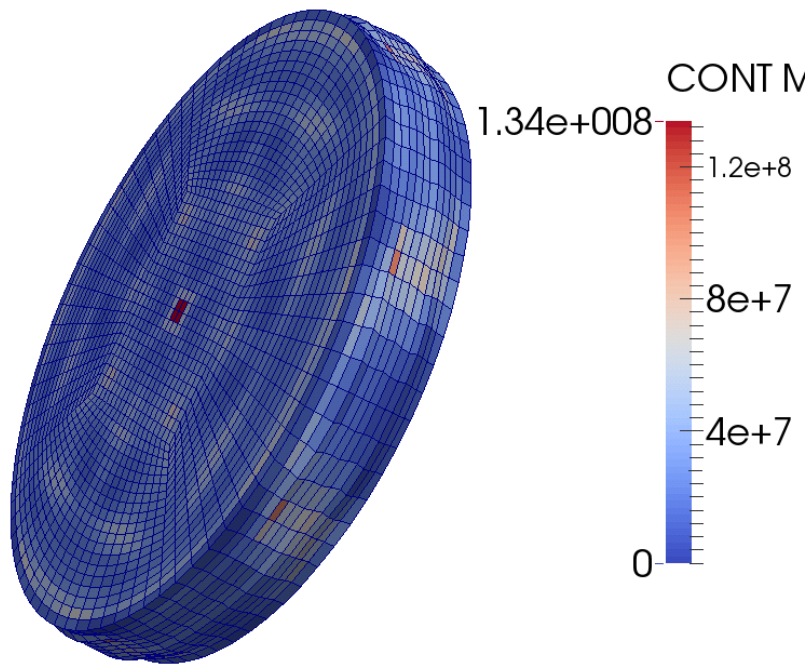


Figure 15: foam_impact5

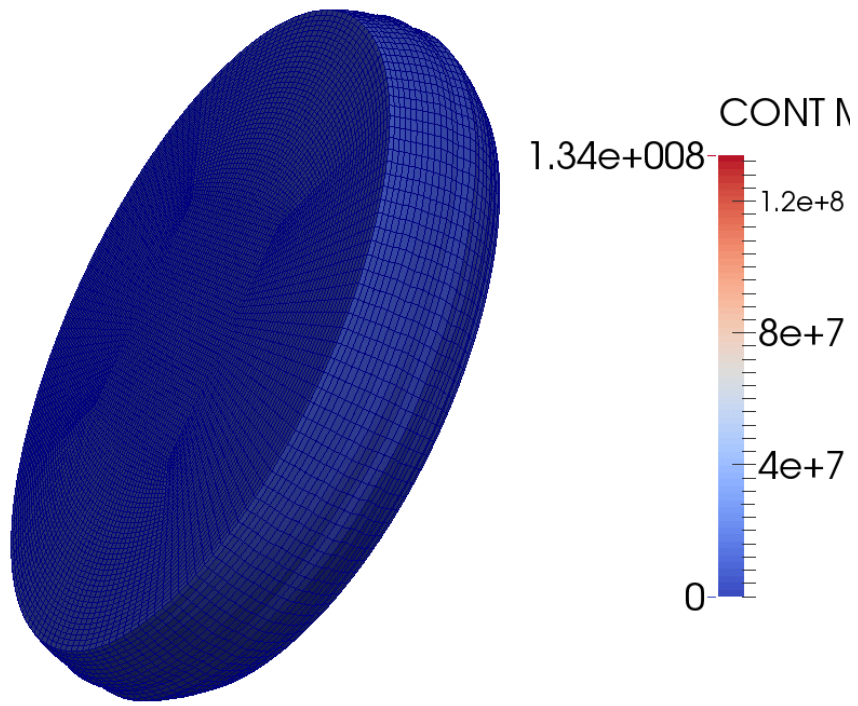


Figure 16: foam_impact6

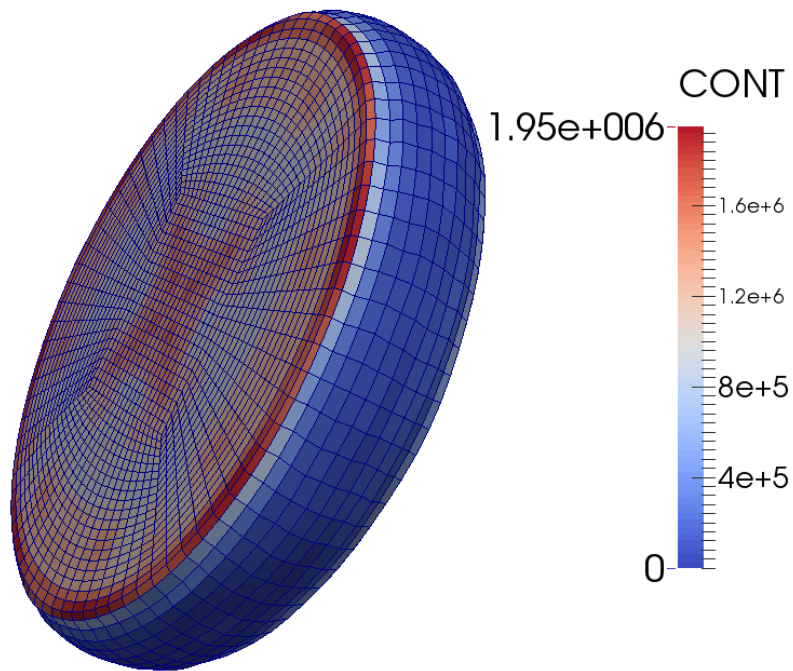


Figure 17: foam_impact7

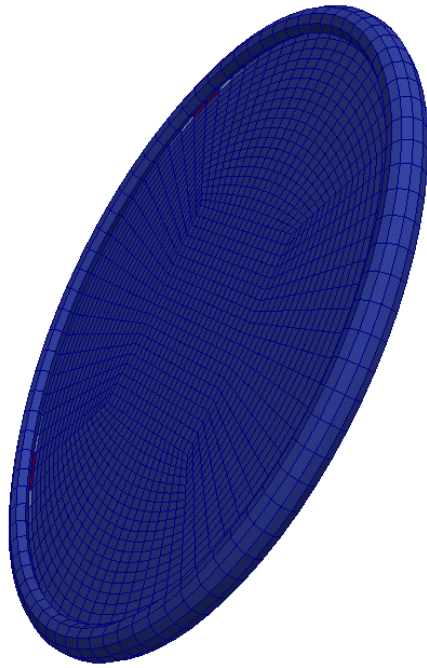


Figure 18: foam_impact8

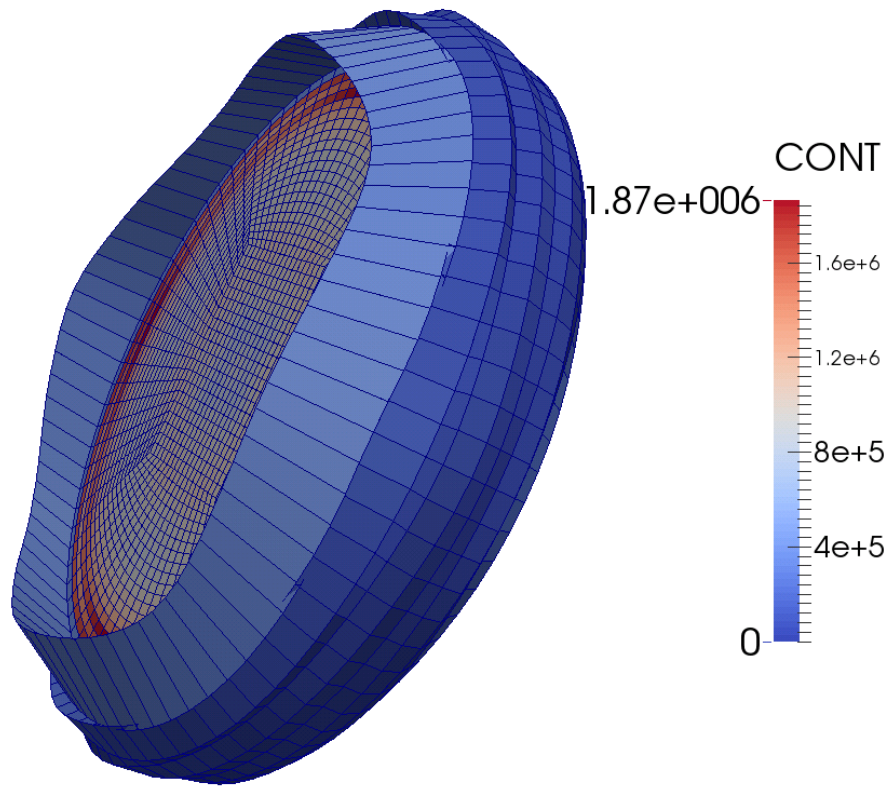


Figure 19: foam_impact9

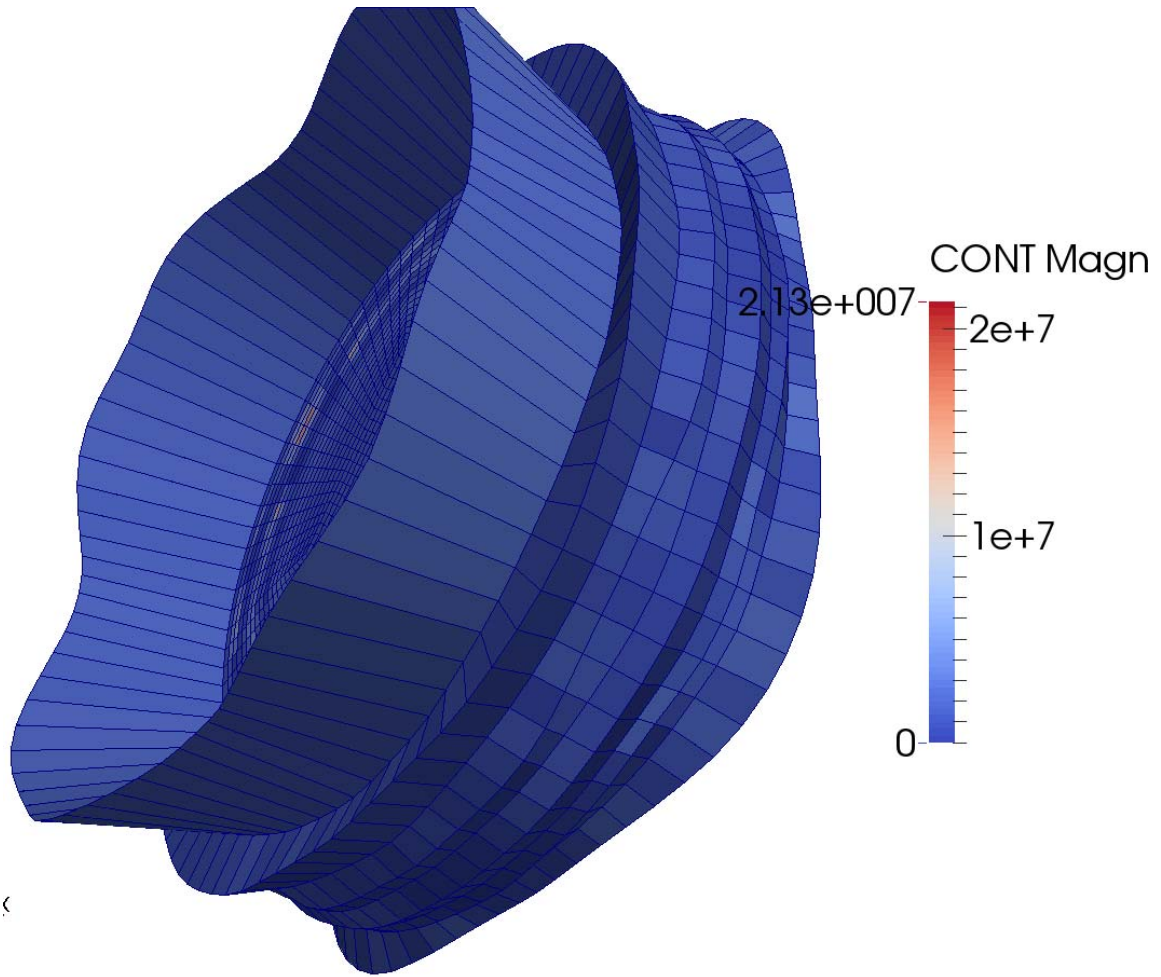


Figure 20: foam_impact10

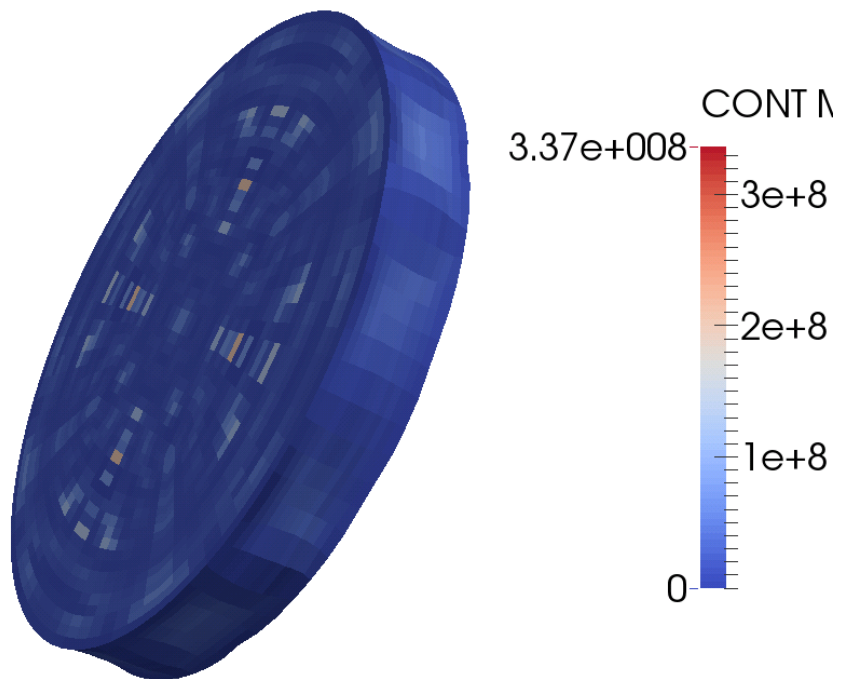


Figure 21: foam_impact11

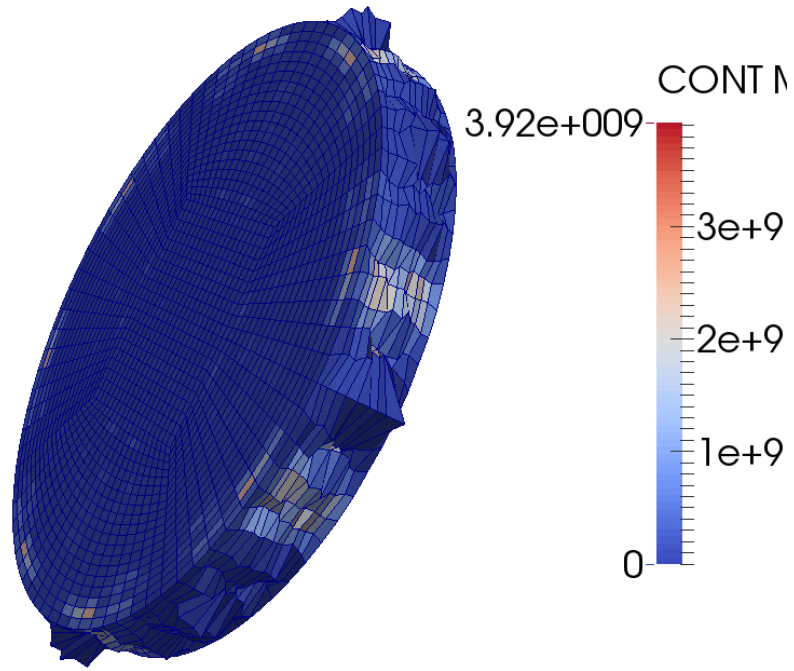


Figure 22: foam_impact12

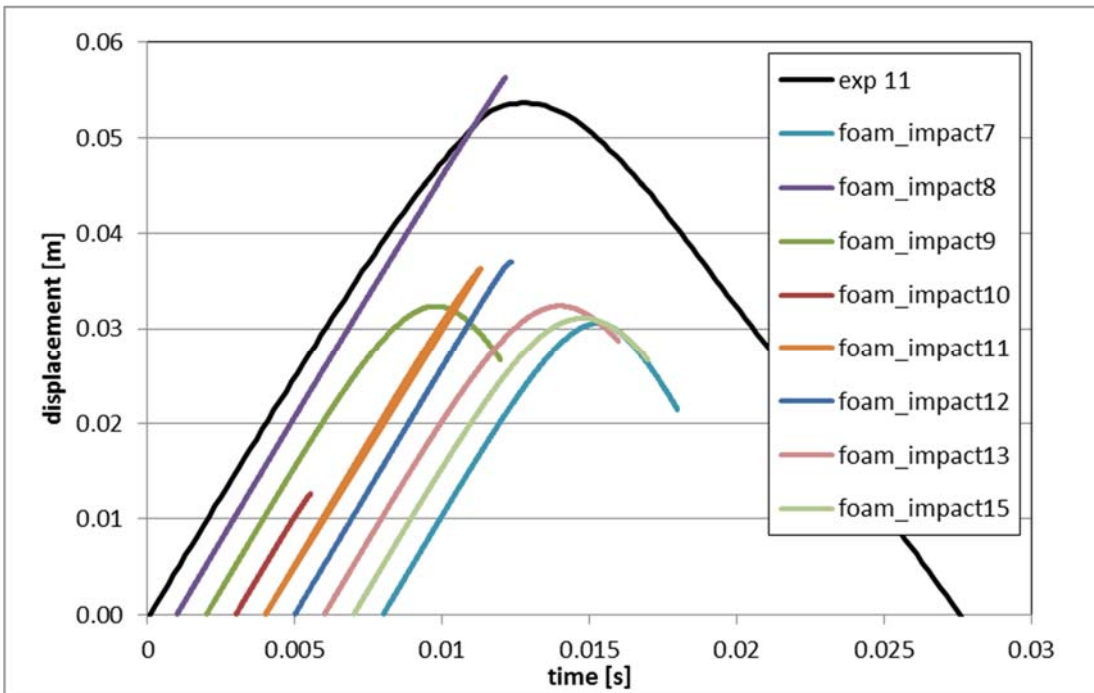


Figure 23: Force history for the models foam_impact7 to foam_impact15

3.2 New material model for sponge foams

The simulations in the previous chapter have shown that also when the force history is represented quite well the displacement history is underestimated significantly. Therefore, it should be reflected if the material law used for these simulations is appropriate.

The hyperelastic material uses some assumptions. The bulk modulus is set to constant. This may be true for small strains but for a foam material under high strains the bulk modulus is most probably not constant. It will increase dramatically when the pores in the foam are compacted. Together with that, the Young's modulus is not constant. Most probably also the Poisson's ratio depends on the strain. The value of it will most probably higher for high hyperelastic strains.

In addition there are some questions about the conformity of the experiment and the numerical model used for the parameter identification. While in the experiment the strains are blocked in lateral directions due to the load plates in the numerical procedure to get the material parameters the strains are calculated under the assumption of a pure 1D experiment (Figure 24). It means for example for a strain of 0.88 the lateral strains in case of the numerical experiment are assumed to be 1.7. In the experiment the lateral strains are much smaller but visible. They are difficult to measure since they are not uniform. In the previous report [9] the lateral deflection of the used foam is measured for one strain stage. At 80 % longitudinal strain the lateral strain could be measured to 0.1. Taking these results the Poisson's ratio can be estimated to 0.08. Due to the non-constant values for the bulk modulus, the Young's modulus and the Poisson's ratio more detailed investigations are needed.

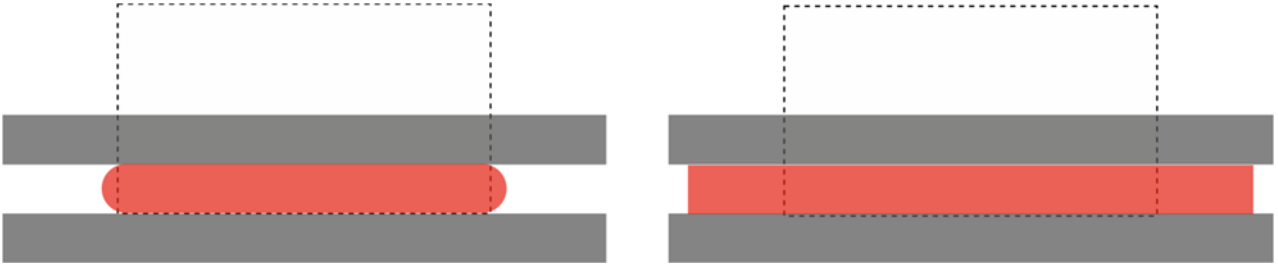


Figure 24: Material experiment (left) in comparison with numerical experiment (right)

3.2.1 Ogden-Storåkers hyperelastic foam

The material law used until now for the foam simulations foresees a constant bulk modulus. This limitation can be overcome by using more appropriate material laws for elastic foam. One is given with the so-called Ogden-Storåkers hyperelastic foam model. It is an enhanced formulation of the classical Ogden formulation

$$W = \sum_{p=1}^N \frac{\mu_p}{\alpha_p} \left(\lambda_1^{*\alpha_p} + \lambda_2^{*\alpha_p} + \lambda_2^{*\alpha_p} - 3 \right) + K (J - 1 - \ln J) \quad (2)$$

with $\lambda_i^* = \lambda_i J^{-1/3}$

Storåkers [16] replaced the bulk modulus of that equation with an additional material parameter set β_p

$$W = \sum_{p=1}^N \frac{\mu_p}{\alpha_p} \left(\lambda_1^{\alpha_p} + \lambda_2^{\alpha_p} + \lambda_2^{\alpha_p} - 3 + \frac{1}{\beta_p} (J^{-\alpha_p \beta_p} - 1) \right) \quad (3)$$

In this equation, the volumetric and the deviatoric parts are combined which can be shown by writing (3) in an expression with λ_i^*

$$W = \sum_{p=1}^N \frac{\mu_p}{\alpha_p} \left(J^{1/3\alpha_p} \left(\lambda_1^{\alpha_p} + \lambda_2^{\alpha_p} + \lambda_2^{\alpha_p} - 3 \right) + 3 \left(J^{1/3\alpha_p} - 1 \right) + \frac{1}{\beta_p} \left(J^{-\alpha_p\beta_p} - 1 \right) \right) \quad (4)$$

As shown by ABAQUS [13] and Schrodtt [15] and Kolling [14] the bulk modulus and the shear modulus for small strains in case of the Ogden-Storåkers material can be calculated by deriving the volumetric part of the energy function and get

$$\mu = \frac{1}{2} \sum_{p=1}^N \alpha_p \mu_p \quad (5)$$

and

$$K = \sum_{p=1}^N 2\mu_p \alpha_p (\beta_p + 1/3) \quad (6)$$

The derivation of equation (3) gives the stresses

$$\sigma_i = \sum_{p=1}^N \frac{\mu_p}{J} \left(\lambda_i^{\alpha_p} - J^{-\alpha_p\beta_p} \right) \quad (7)$$

The current stiffness must be used to determine the sound speed for the critical time step size. It can be got by the derivation of the formula for the stresses. The stresses are defined in the principle directions. Therefore, the direction with the highest strain will be used for this step. The stress formulation reduces to

$$\frac{d\sigma_i}{dJ} = \sum_{p=1}^N \frac{\mu_p}{J} \alpha_p \lambda_i^{\alpha_p-1} + \sum_{p=1}^N -\frac{\mu_p}{J^2} \lambda_i^{\alpha_p} \lambda_j \lambda_k - \sum_{p=1}^N \mu_p J^{-2-\alpha_p\beta_p} (-1 - \alpha_p\beta_p) \lambda_j \lambda_k \quad (8)$$

This can be simplified to

$$\frac{d\sigma_i}{dJ} = \sum_{p=1}^N \frac{\mu_p}{J^2} \left(J^2 \alpha_p \lambda_i^{\alpha_p} - \lambda_i^{\alpha_p} + J^{-\alpha_p\beta_p} (1 + \alpha_p\beta_p) \right) \quad (9)$$

The Ogden-Storåkers material model can be used for highly compressible materials.

3.2.2 Examples

The newly implemented material law (MAT HYPE TYPE 5) is used to redo the already presented calculation of the elastic foam impact (Table 10).

Table 10: Parameter identification for a specific rubber: parameters for TYPE 5 calculations

	Nb elem. Circumf er.	Nb elem. thickne ss	Speed	Material	Comments
foam_impact 17	40	6	5.2	MAT_HYPE 5	
foam_impact 19	40	8	8.7	MAT_HYPE 5	
foam_impact 20	80	8	5.2	MAT_HYPE 5	
foam_impact 21	80	8	8.7	MAT_HYPE 5	

It can be seen that the displacement history can be well represented by the new material model. The very last loading of the material is slightly too stiff, i.e. rebound starts too early. This could be due to the limited material experiments especially at that state of the material.

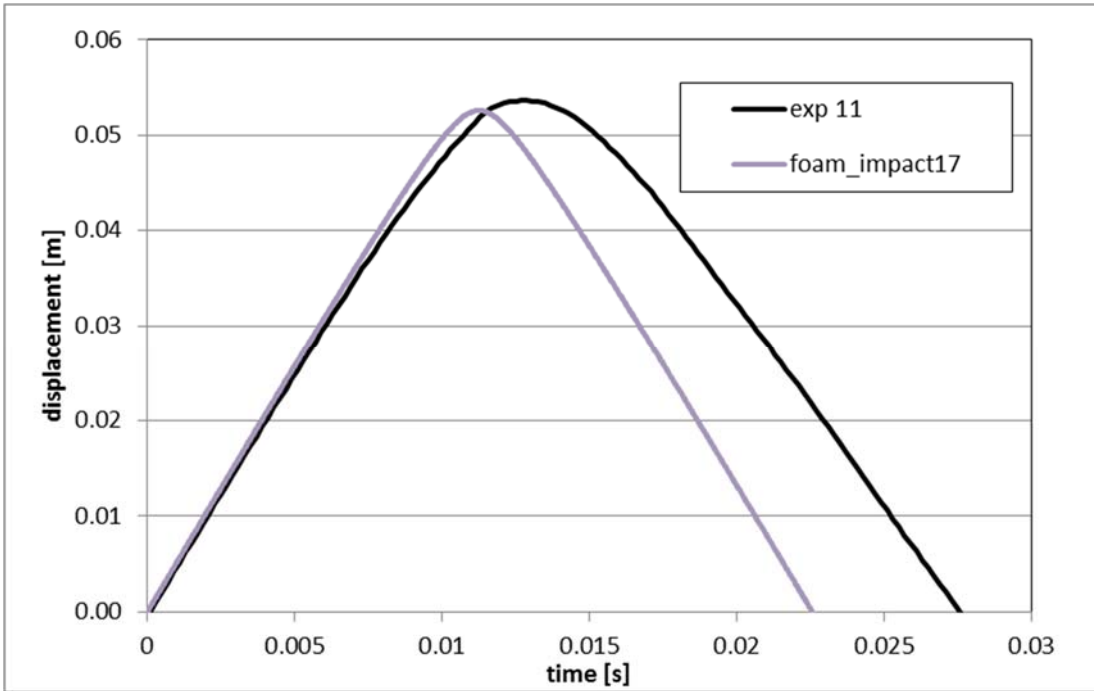


Figure 25: Force history for the model foam_impact17, slower impact (MAT HYPE TYPE 5)

The displacement history of the faster experiment can also much better be described by the new elastic foam material as it can be seen in Figure 26.

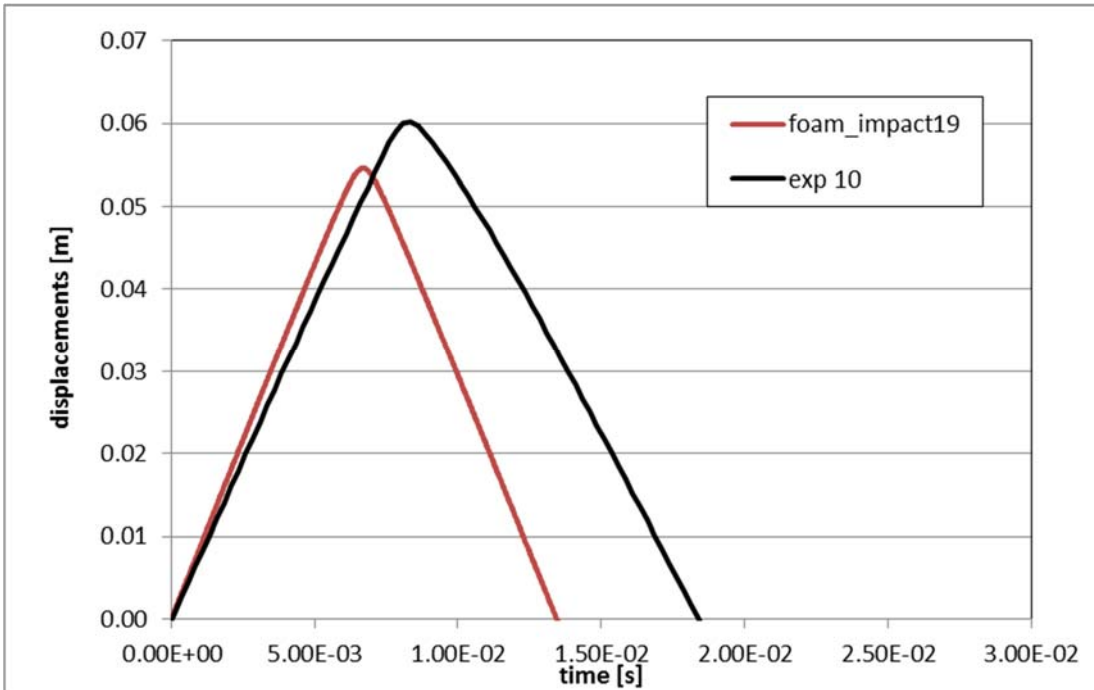


Figure 26: Force history for the model foam_impact19, faster impact (MAT HYPE TYPE 5)

It can be concluded that the standard hyperelastic material laws are not usable for elastic foams since the Young's modulus is set to constant. The additional terms of the Ogden-Storåkers-formulation gets much more precise results and should be used in the

4 Numerical results

The objective of this chapter is to present the results of the numerical simulations and compare them with the experimental ones. This is a process where the simulation tries to verify the experimental data. Since this set of experiment is among the first ones, there are many uncertainties in both experimental data and simulation results. At the end of this section, some remarks are pointed out trying to highlight where the simulation agrees with the experimental data and to justify the discrepancies.

Three tests took place in the laboratory where the velocity of the impacting mass is changing. In all the experiments the same specimen has been used. The first test is not considered for the simulation since the contact of the impacting mass and the specimen was not plane as depicted in Figure 27. This problem was fixed in the next two successful tests. The experimental results obtained from the tests was the displacement and the velocity of the impacting mass, the measured loads on the load cells (three on the aluminium plates and two on the support points) and the displacement of the specimen. The velocities and the displacements in the tests have been calculated with optical devices.



Figure 27: Pinballs of the contact bodies

4.1 Blast 15

In the “Blast 15” experiment a fragile notched bolt with 8mm diameter has been used in order to hold the spring in the blast actuator. The velocity of the impacting mass the moment that gets in contact with the specimen is 6.2 m/s and that is the input velocity for the simulation. For the outputs of the numerical simulation, the “REGI” directive has been used in order to obtain an average value for the object under consideration. So for example for the velocity of the impacting mass the steel mass part has been considered as a group and the average value of all its nodes is giving much smoother results than taking one point. Especially, for the experimental velocity curves a lot of noise is imported since they are calculated from the differentiation of the displacement curve.

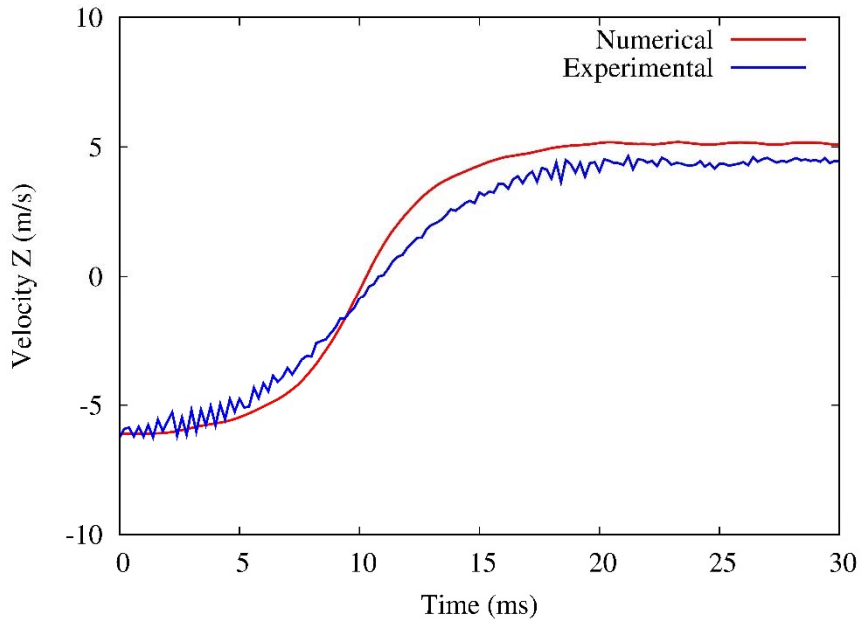


Figure 28: Velocity of the impacting mass

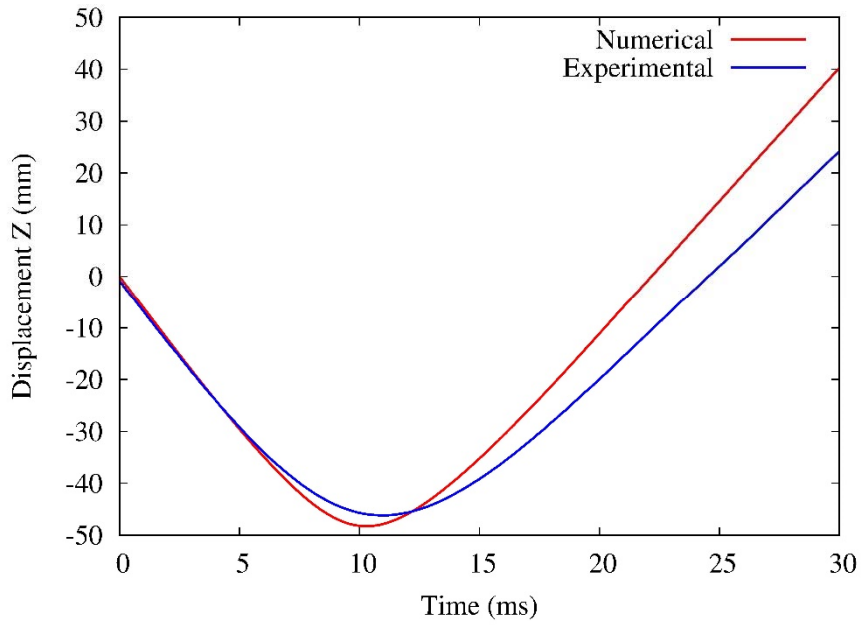


Figure 29: Displacement of the impacting mass

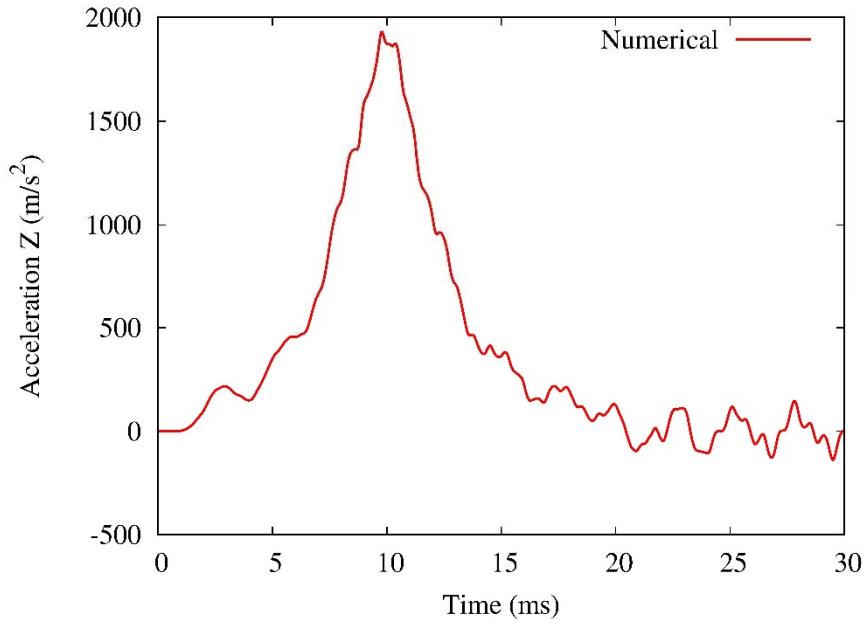


Figure 30: Acceleration of the impacting mass

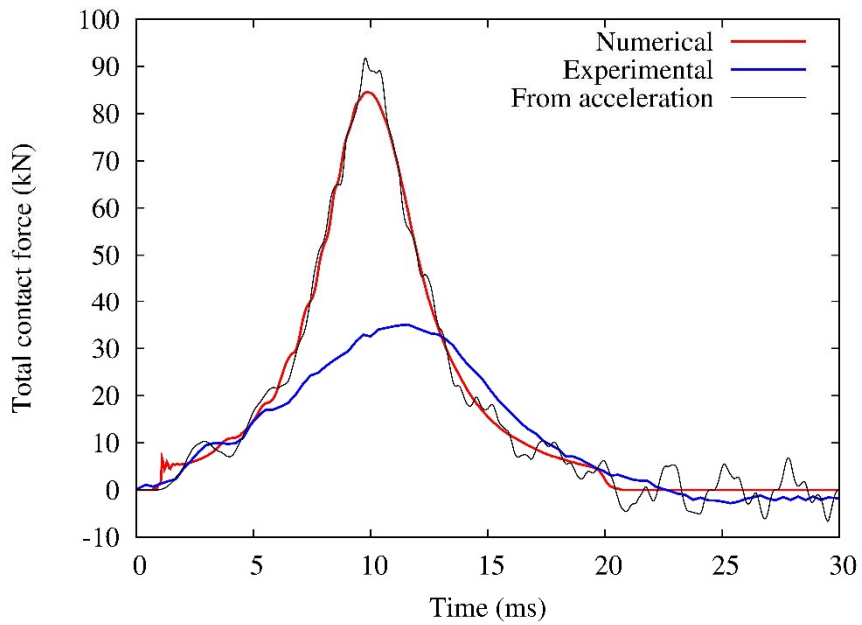


Figure 31: Total contact force of the impacting mass

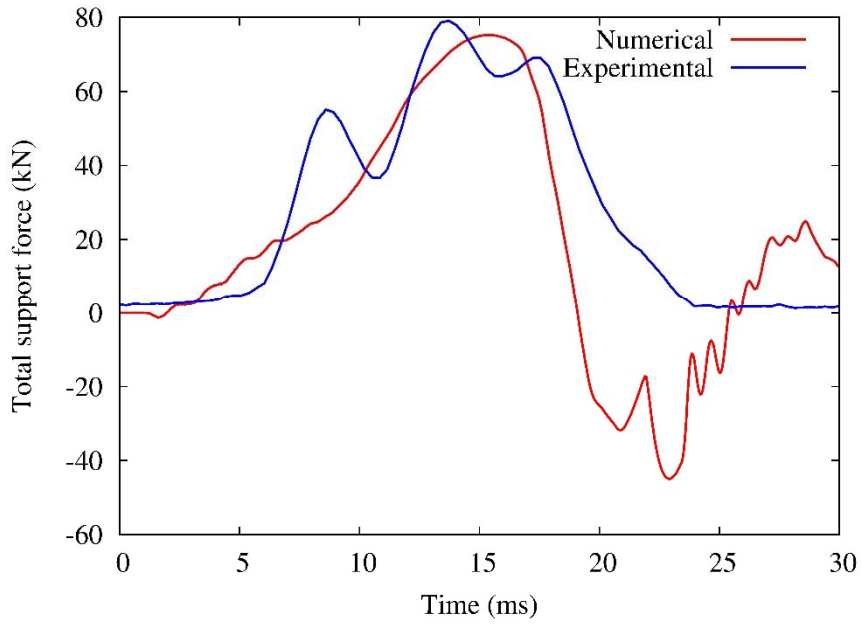


Figure 32: Support forces

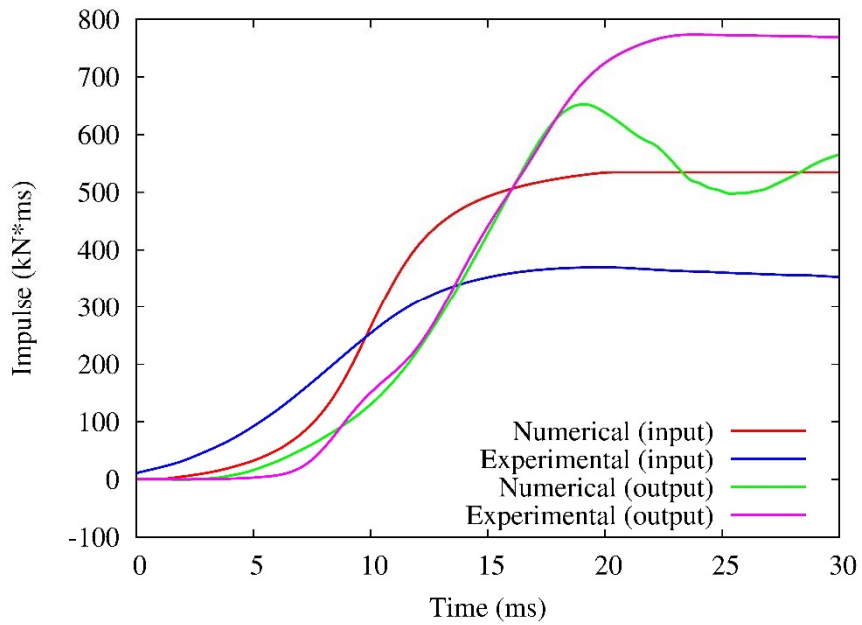


Figure 33: Input and output impulse

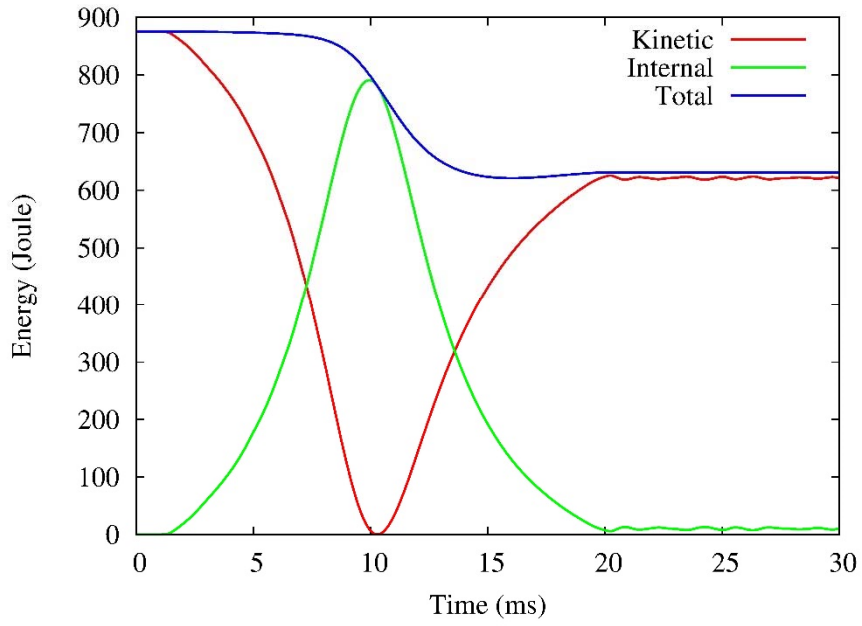


Figure 34: Energy of the impacting mass

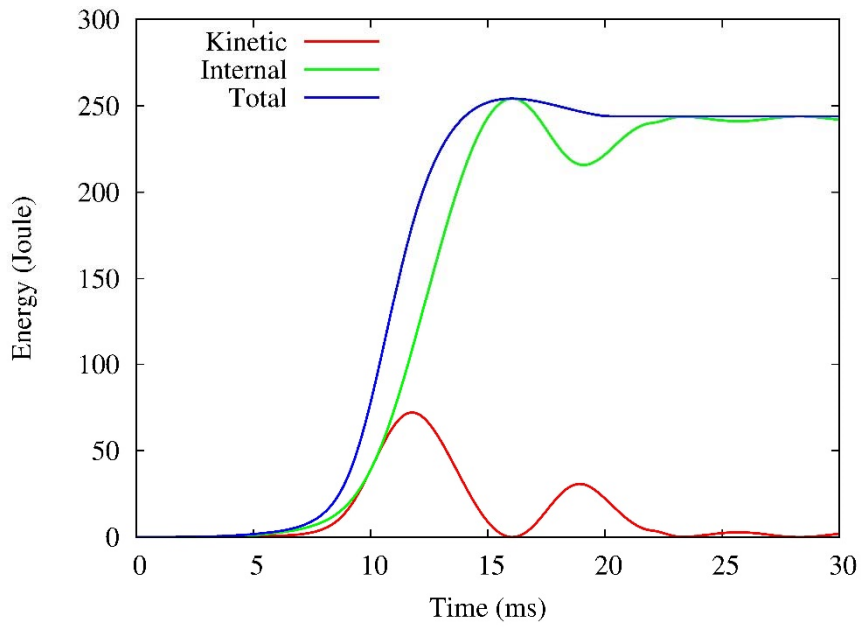


Figure 35: Energy of the specimen

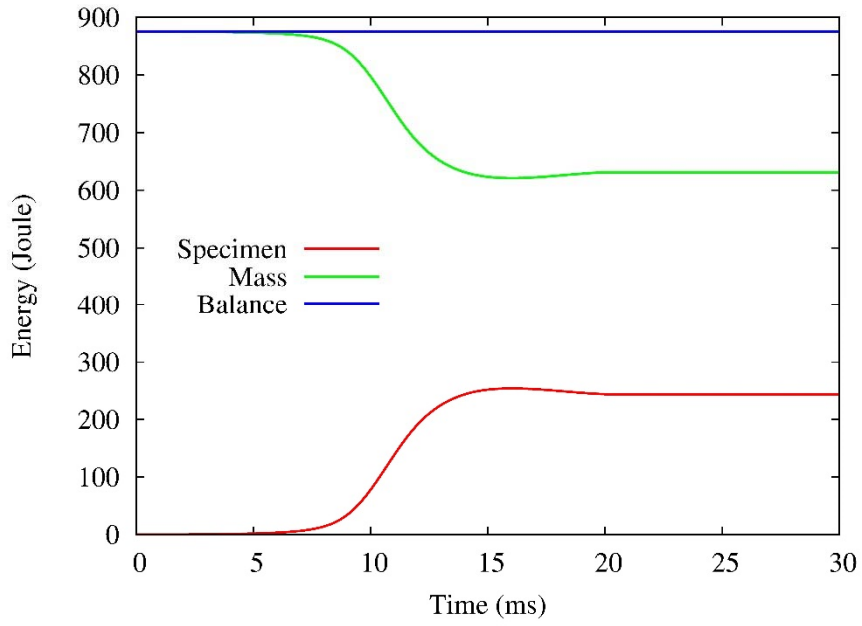


Figure 36: Energy balance

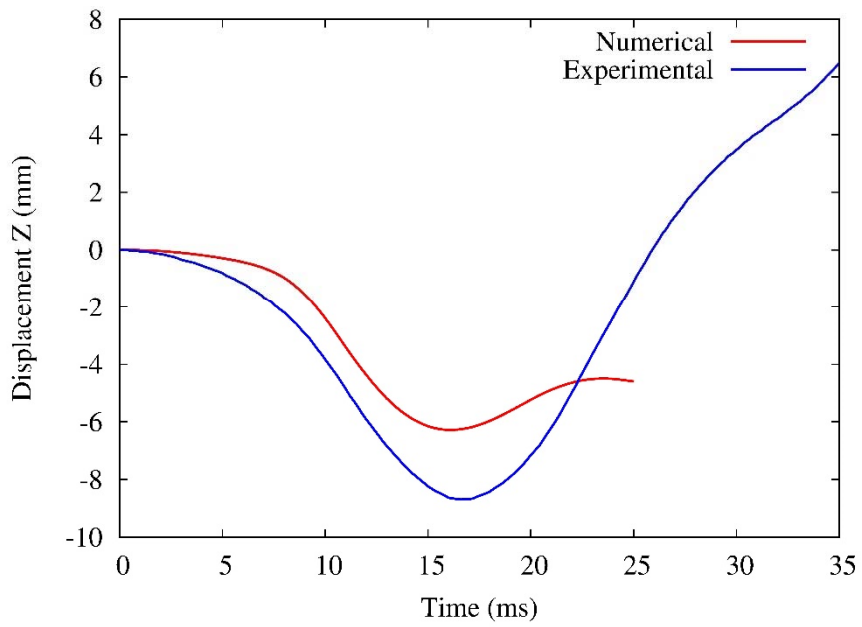
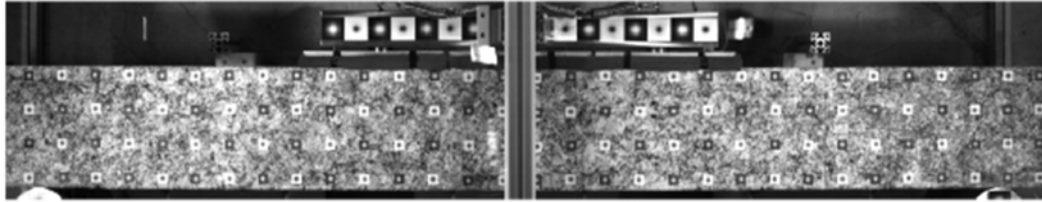
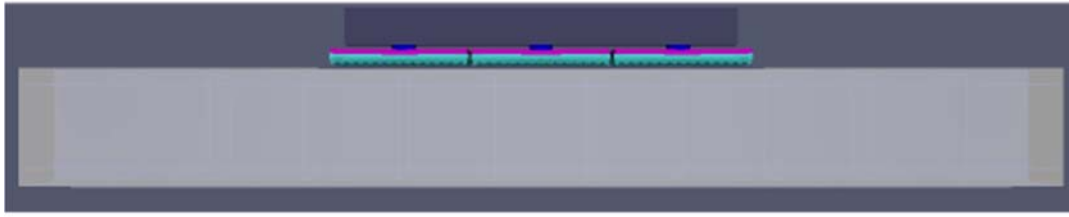


Figure 37: Vertical displacement of the column

Numerical



Experimental

Figure 38: Comparison of numerical and experimental model for the time instant where the velocity of the impacting mass is zero

Figure 28 presents the velocity of the impacting mass (vertical to the specimen) for both numerical and experimental data. As already mentioned in the experimental curve there are some oscillations related to the fact that it is obtained after the differentiation of the displacement curve. It can be observed that there is a good accordance between the two curves. The velocity of the impacting mass after the rebound in the numerical output is a little higher than the experimental one while also the curve is a little stepper. This discrepancy is due to the material law used for the simulation of the elastic foam material. It is very difficult to obtain accurate results for the elastic foam material since there are many parameters of uncertainties such as the input stress-strain curve from the laboratory and the calculated coefficients for the best fit of the used equation to that curve. It should be noted that several attempts have been made in order to optimize the simulation of the elastic foam and it can be pointed out that this level of accuracy is sufficient [9].

Figure 29 presents the experimental and the numerical displacement of the impacting mass (vertical to the specimen). The results are similar to the previous paragraph where the maximum displacement is a little higher in the case of the numerical results and the inclination of the curve in the rebound phase is steeper. The accordance of the results is satisfying and a very important aspect is that the duration of the phenomenon is more or less around 20ms for both cases. This is an indicator that the selected material law for the elastic foam material is good enough since in the first approaches the duration of the phenomenon in the numerical case was much smaller.

Figure 30 shows the average acceleration of the impacting mass for the numerical case. There are no data for the experimental case since no accelerometers were included in the experiment. In the next experiments it is very possible to use accelerometers on the impacting since the acceleration data can verify the results from the load cells. Figure 31 presents the numerical and the experimental results for the impacting force. The experimental data are obtained from the load cells while the numerical data are calculated after the addition of all the contact forces on all the involved nodes. A comparison of the two curves shows that the duration of the impact is the same and although the shape of the curve is similar the peak value in the case of the numerical simulation is much higher (3 times). The numerical value can be verified also from the acceleration curve since the multiplication of the acceleration curve with the mass of the impacting device is giving similar results. The calculation of the contact force curve is very important since from the peak force (pressure) and the impulse the equivalent blast data (mass of explosive material and standoff distance) can be obtained.

Unfortunately, the absence of experimental acceleration data does not allow to claim if the actual impact force is closer to the one measured in the load cells or the one calculated from the numerical simulation. However, some aspects can introduce erroneous results in both cases. In the case of the numerical simulation, the elastic foam material law is under development and there are a few inaccuracy sources. The model seems to work in a realistic way but the

coefficients used for the interpretation of the foam behaviour has been done with a best feet procedure [9] and this procedure is not optimized yet. Maybe a better calculation of the desired coefficients can give different results. On the other hand, the measured force on the load cells in the experimental device has not been verified yet. The impacting force is passing through the aluminium plate before entering in the load cell and it is very possible that the aluminium plate is filtering the measured force.

Figure 32 presents the support forces for both cases. The experimental data are obtained from the load cells located between the support of the specimen and the reaction wall. The numerical results are obtained from the addition of all the support forces on the nodes that the blockages have been put. There are many similarities in the two curves, the duration is more or less the same while also the peak force is very close in the two cases. It should be noted that in the numerical simulation the support is a simple blockage in the vertical direction which prevents the specimen from moving in both ways, while in reality the support stops the specimen only in one way (towards the reaction wall) and it is free to move in the other way. This already can justify some of the discrepancies between the two curves. A future numerical simulation with a more realistic representation of the boundary conditions will give more accurate results.

Figure 33 shows the numerical and the experimental results for the input and the output force impulse in the experimental apparatus. The input impulse is calculated from the integration of the contact force of Figure 31 while the output impulse is calculated from the integration of the support force of Figure 32. The impulse expresses the change of the momentum of the system which for the numerical case is $47.6\text{kg} * (6.2 - (-5.1))\text{m/s} = 537.88\text{kg}\cdot\text{m/s}$ or $\text{kN}\cdot\text{ms}$. The comparison of the input and the output impulse is taking place in order to see if there are and kind of losses during the experiment. For the numerical results, the two curves (red and green) are having similar final value as expected, while in the case of the experimental data the two curves (blue and magenta) are having different final value. It is also strange that the impulse of the output is much higher than the input, a fact that is not normal (the opposite can be expected in the case of any energy loss in the collision). This difference enhances the hypothesis that the load cells might not measuring correctly the forces on the apparatus.

The next three figures present the energy distribution in the experimental configuration and the curves corresponds to the numerical data. Figure 34 depicts the energy status in the impacting mass. First, the impacting mass has only kinetic energy that during the impact is transformed into strain energy mainly on the elastic foam layer. At the rebound phase, the impacting mass has only kinetic energy lower than the initial one since one part of it has gone to the specimen. Figure 35 presents the energy check in the specimen, where in that case, there is an oscillation of the kinetic energy until the specimen rests. There is no plastification of the reinforcement and a minor plastification of the concrete part. Figure 36 depicts the energy balance in the system.

Figure 37 presents the deflection on the middle of the specimen for both numerical and experimental cases. In the experimental data, the displacement after the 25ms is still increasing and this is because the specimen moves in that direction after the impact as a rebound phase since there is nothing to keep it in the initial position. The maximum deflection of the specimen is underestimated in the numerical case while the permanent deflection is higher than the experimental value (although it is not easy to identify the experimental value from the figure since the specimen is moving after the impact). In addition, the period of the oscillation in the case of the numerical value is lower which means that the material properties are not very accurate. The main reason of the differences of the results is the fact that the material properties for both concrete and steel were not provided by the constructor and typical values have been selected. In the future the laboratory will be able to provide more accurate data on the material properties of the specimen after certain tests. At that point, the numerical simulation is not focused on the results on the specimen but on the results of the impact (contact force and impulse) between the mass and the column. Figure 38 compares the photograph from the laboratory with the paraview output [6] from the numerical simulation, for the moment that the impacting mass has zero velocity.

4.2 Blast 16

In the “Blast 16” experiment, a fragile notched bolt with 9.25mm diameter has been used and this resulted into producing higher impact velocity. The velocity of the impacting mass the moment that gets in contact with the specimen is 12 m/s and that is the input velocity for the simulation. This as a more severe case where the damage on the column is evident. The way that the results are presented is similar to the previous experiment.

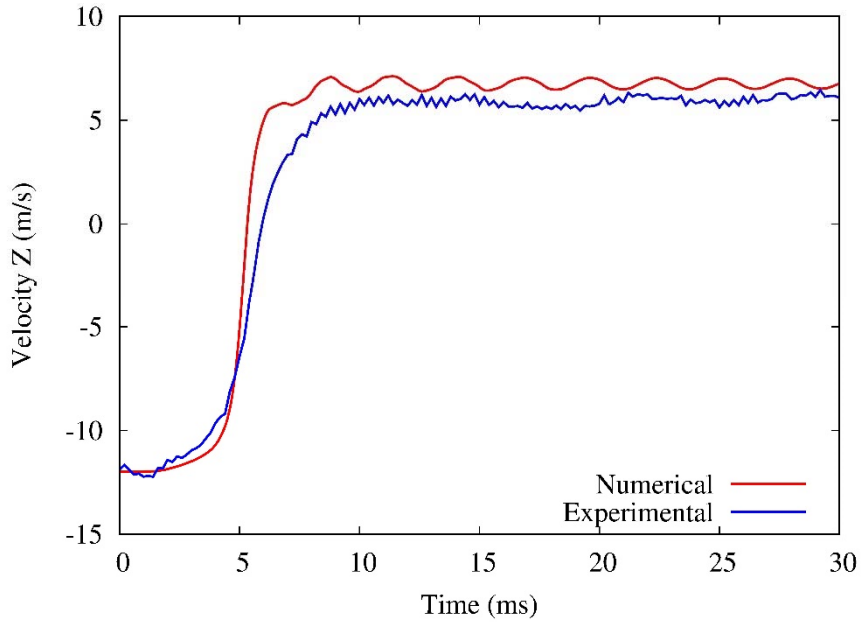


Figure 39: Velocity of the impacting mass

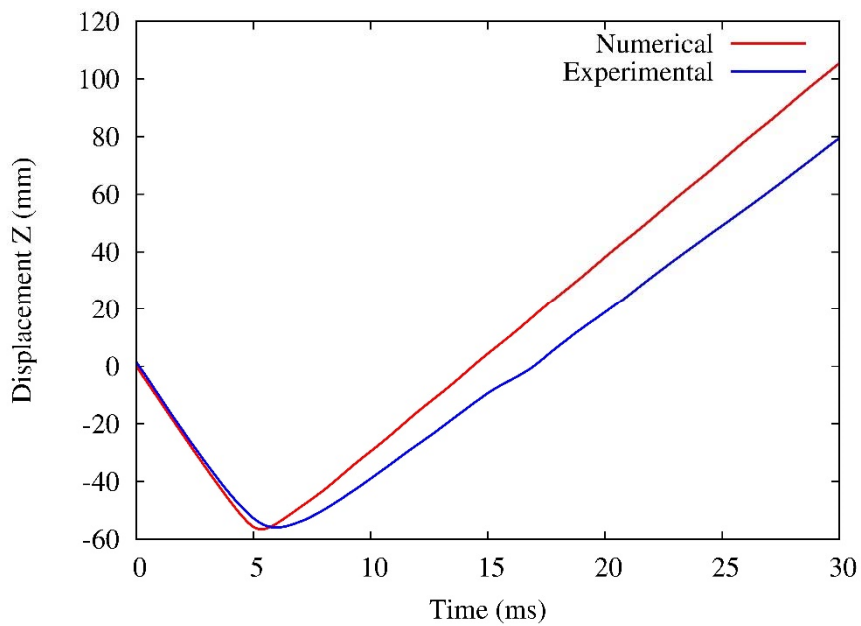


Figure 40: Displacement of the impacting mass

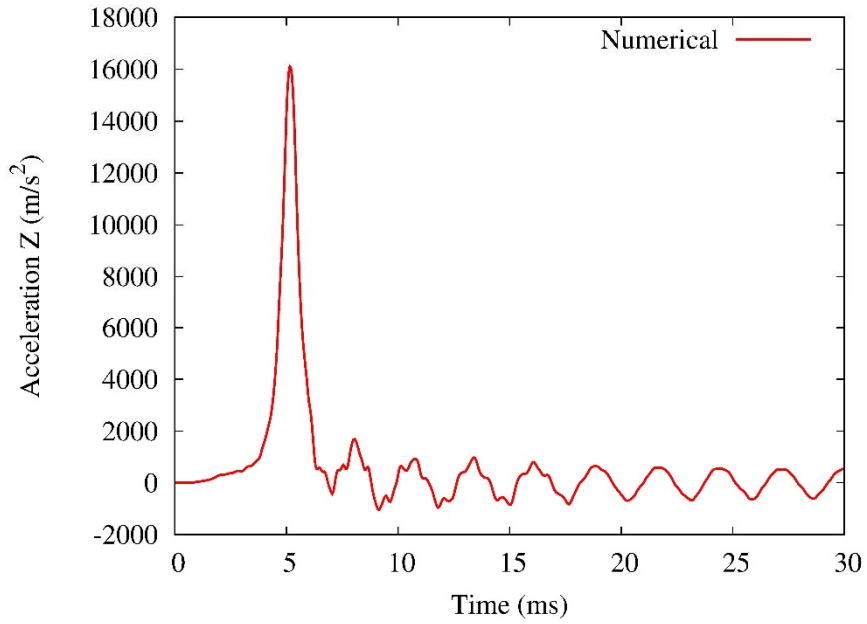


Figure 41: Acceleration of the impacting mass

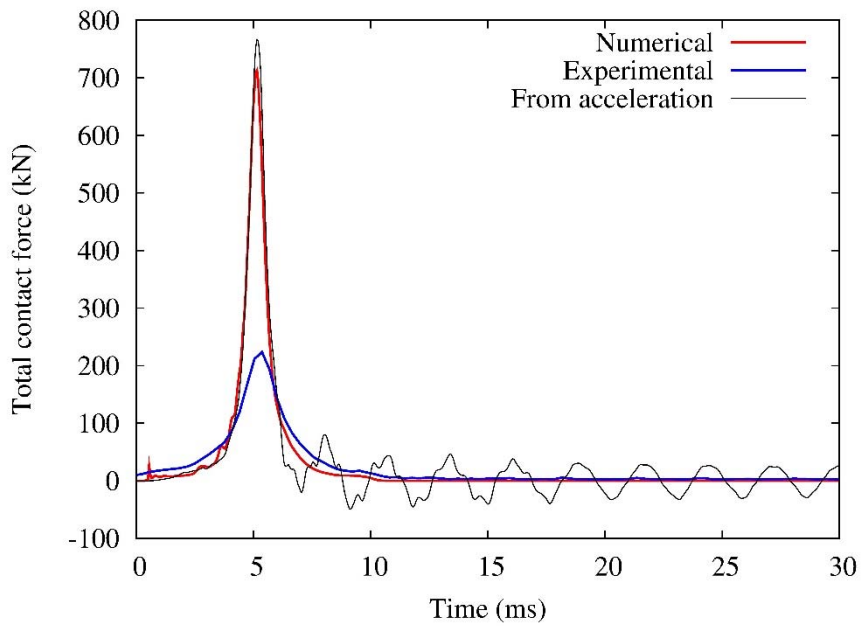


Figure 42: Total contact force of the impacting mass

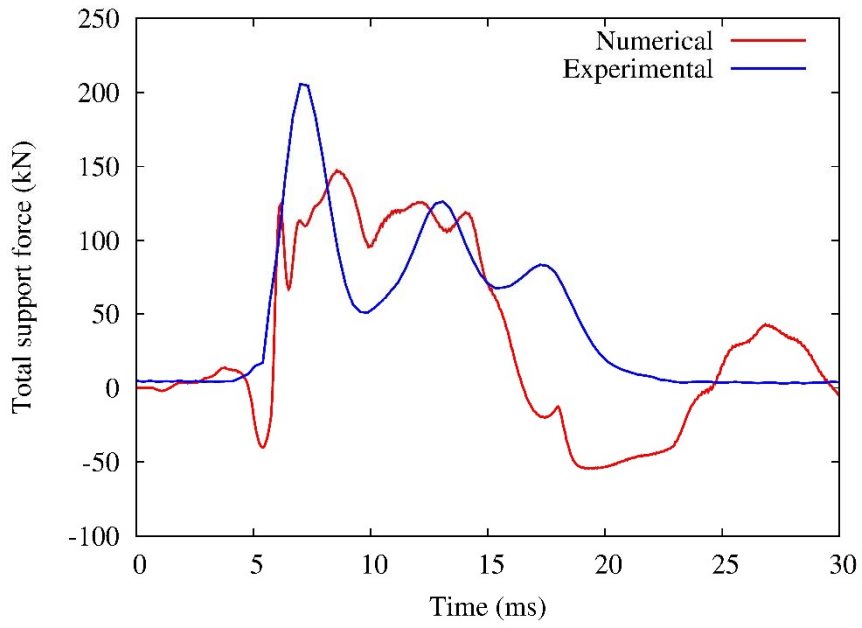


Figure 43: Support forces

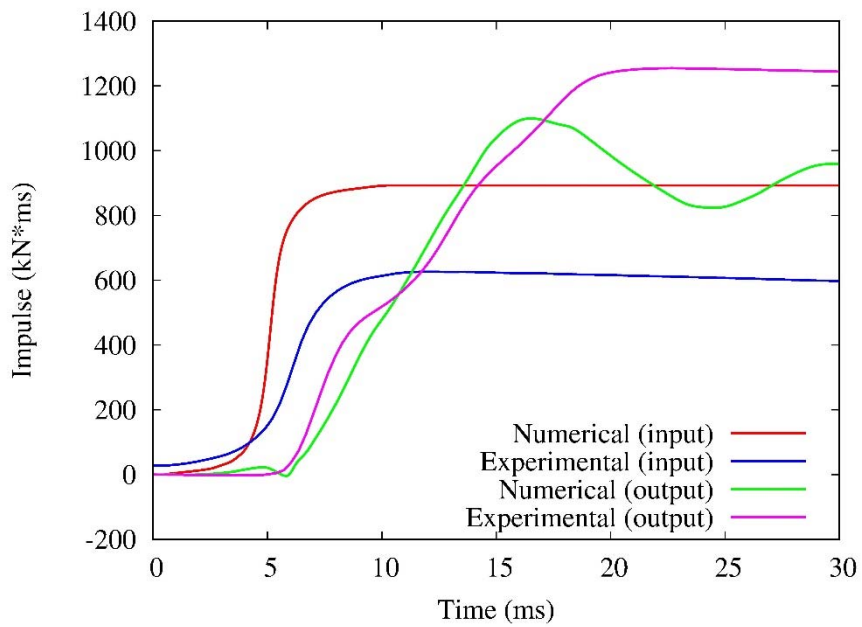


Figure 44: Input and output impulse

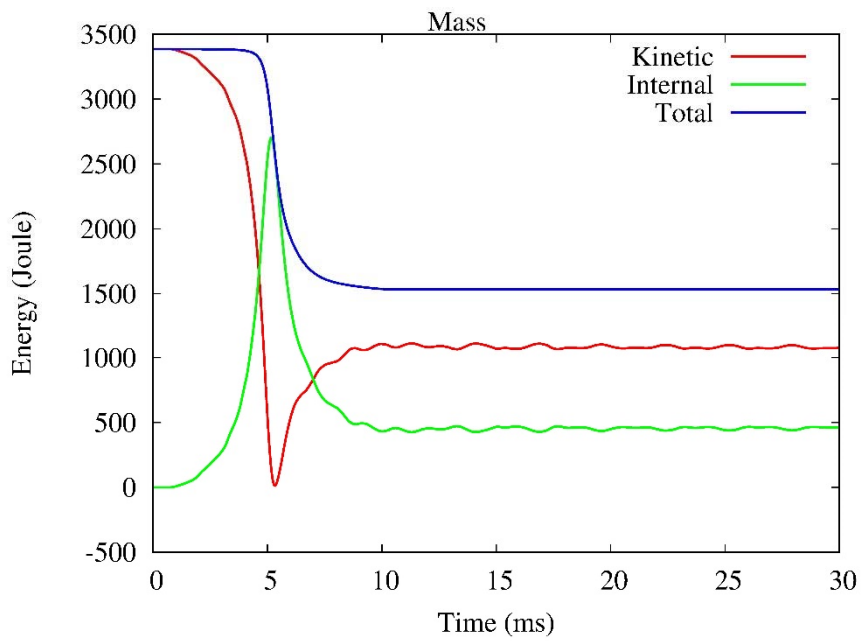


Figure 45: Energy of the impacting mass

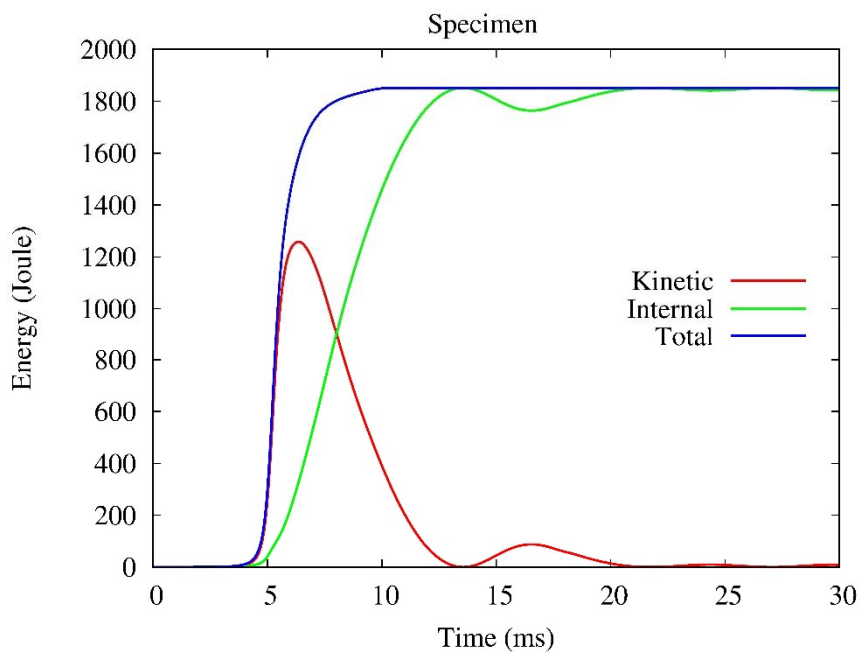


Figure 46: Energy of the specimen

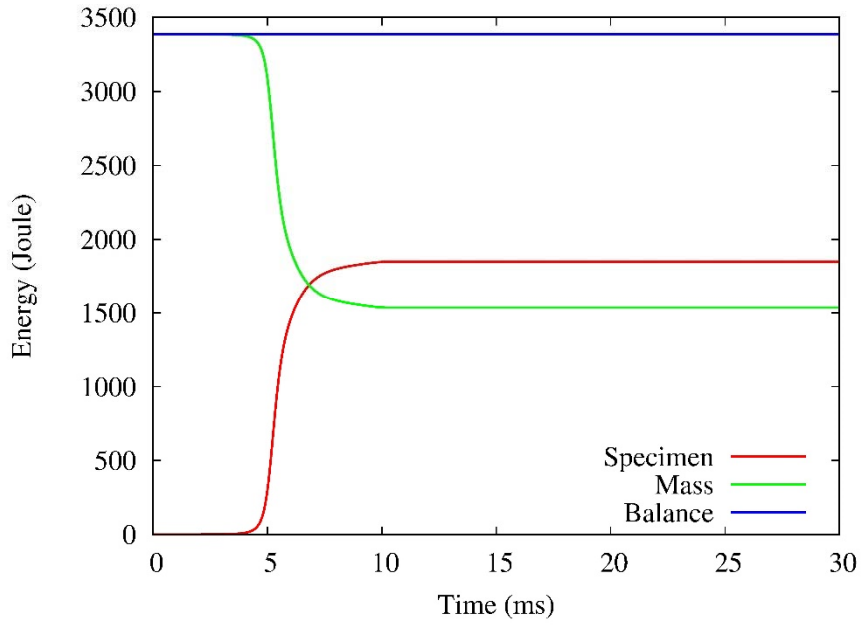


Figure 47: Energy balance

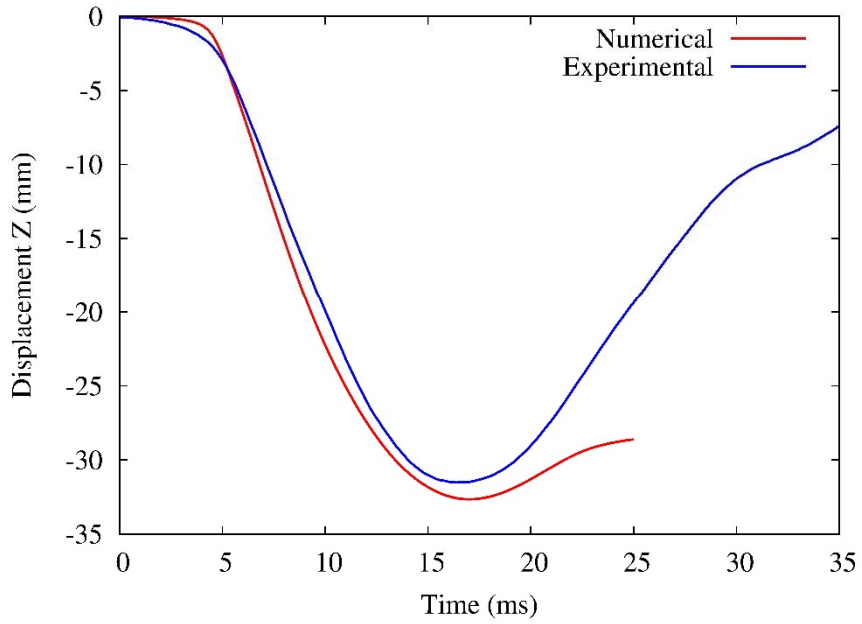


Figure 48: Vertical displacement of the column

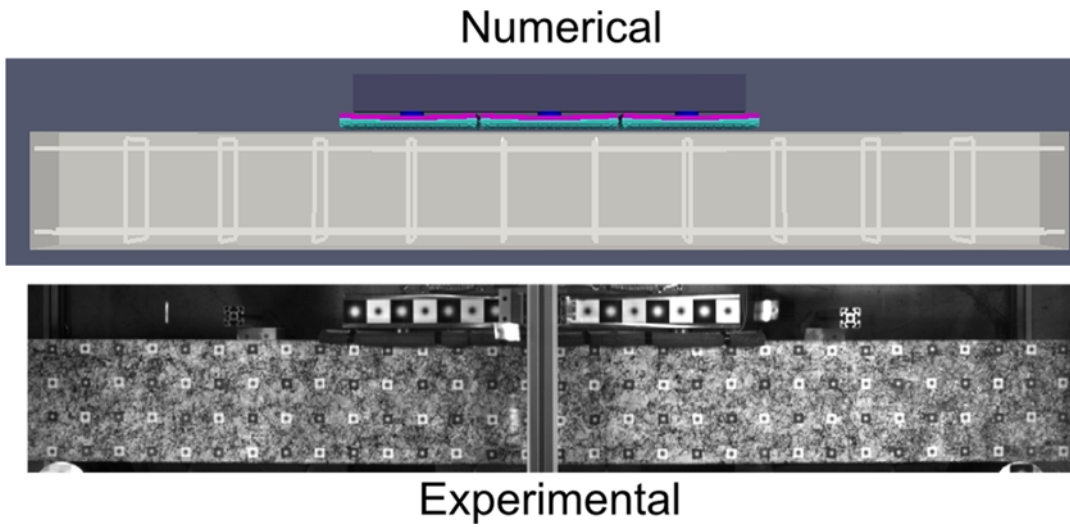


Figure 49: Comparison of numerical and experimental model for the time instant where the velocity of the impacting mass is zero

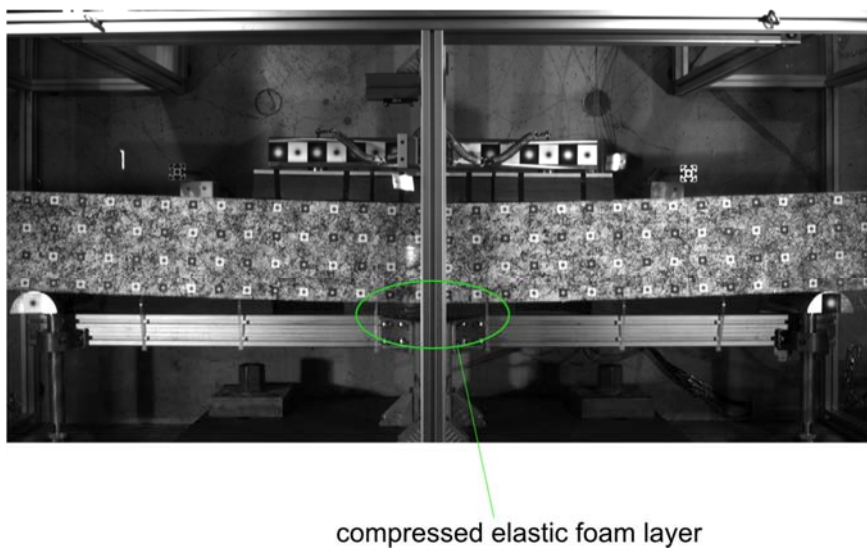


Figure 50: Maximum deflection of the specimen and the compression of the elastic foam layer on the rear part

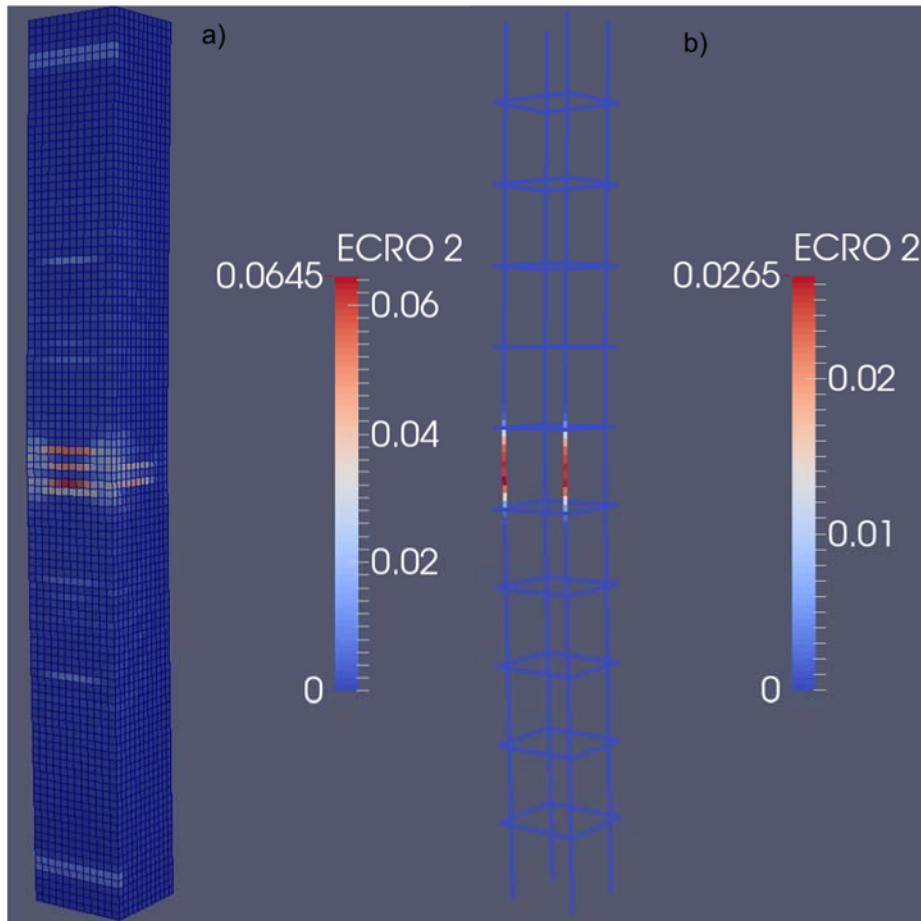


Figure 51: a) Concrete plastic strain b) steel reinforcement plastic strain

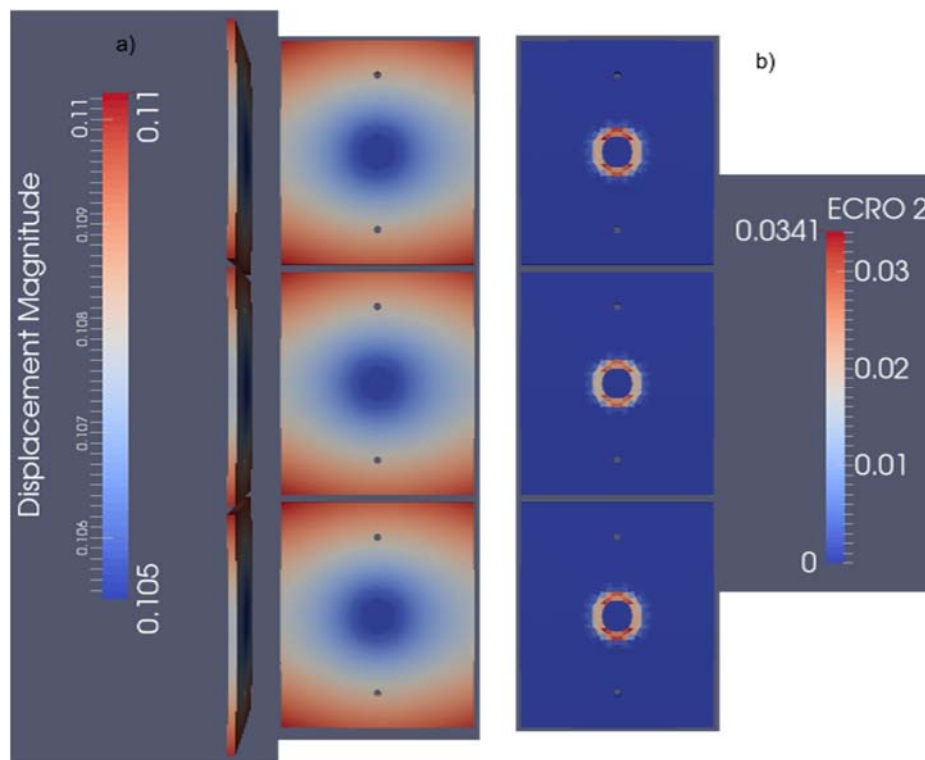


Figure 52: Aluminium plates a) deformation and b) plastic strain

Figure 39 presents the velocity of the impacting mass for the two cases. There is a good accordance of the results between the numerical and the experimental data. The rebound velocity after the impact is a little higher in the case of the numerical data. The curve in the phase where the velocity is changing abruptly is steeper in the numerical case as in the previous experiment. However, in that case there is a better fit between the numerical and the experimental curves. Similar conclusions can be made from Figure 40 where the displacement of the impacting mass is depicted. The maximum displacement of the impacting mass is almost the same for both cases while the inclination of the curve in the rebound phase is steeper in the numerical output.

Figure 41 presents the average acceleration of the steel part of the impacting mass for the numerical case only. Figure 42 depicts the contact force from the load cells for the experimental case. For the numerical part there is one curve (red) that shows the calculated contact forces between the two impact bodies and one curve (thin black) that shows the force calculated after the multiplication of the acceleration with the mass of the impacting part. The duration of the phenomenon is similar (around 10ms) for both numerical and experimental outputs while there is a big difference in the peak value. The conclusions are similar to the ones that pointed out in the previous section. It is not clear which curve is the correct one since on the numerical part there are some uncertainties in the representation of the elastic foam and on the experimental part there is the possibility that the aluminium plates (that are between the specimen and the load cells) are filtering the measured force. It is obvious that a measurement on the acceleration of the impacting mass in the next experiment will give an answer to the dispute.

Figure 43 presents the forces on the support of the specimen. A comparison of the two curves shows that the duration of the phenomenon and the magnitude of the forces is close in the two cases. The profile of the two curves is not the same and this is because the representation of the support in the numerical simulation is different from the experimental especially in the rebound phase of the specimen as described in the previous section. Figure 44 presents the input (of the contact forces) and the output (of the support forces) impulse of the numerical and the experimental data. As in the previous case for the numerical case, there is an accordance in the final value between the input and the output impulse. Both impulses are reaching the expected value ($12\text{m/s} - (-6.7\text{m/s}) * 47\text{kg} = 879\text{m} * \text{kg/s}$ or kNm/s) since the impulse expresses the change in the momentum. In the experimental data, there is a big difference between the input and the output impulse and no one of them is reaching the expected value. It is very possible that the load cells that measuring the impact force underestimate the force and the impulse while in the output case the opposite occurs.

The next three figures show results on the energy quantities for the numerical data. The initial kinetic energy of the impacting mass is transformed into internal energy on the elastic foam layer and then again to kinetic energy. A part of the energy is transported in the specimen while there is a part of energy stored in the aluminium plates after their plastification Figure 52. The aluminium plates after the impact they have been deformed with a residual deflection of 2mm. It is advisable to rethink the design of that part of the apparatus since more severe tests will deteriorate the state of the plates and will produce inaccuracies on the applied load. The kinetic energy on the specimen after the collision is higher in that test while the part of energy that transported in the specimen is higher than the remaining energy on the impacting mass.

Figure 48 presents the maximum deflection of the specimen. The point under consideration is located in the middle of the column. The experimental data as in the previous section are not accurate at the rebound face since the specimen is moving from the original location. A comparison of the two curves shows a good accordance between the experimental and the numerical data. The maximum displacement is very close for both approaches while also the period of the two curves is similar. The remaining deformation of the specimen is not easy to identify from that curve since the concrete column rebounds after the impact. This accordance shows that the numerical simulation of the reinforced concrete column is on the correct way and that using the newly developed material model "DPDC" is a promising option.

Figure 50 presents the top view of the experimental test for the moment that the column has the maximum deflection. It can be observed that the rear part of the column with the maximum displacement is in contact with the elastic foam layer that has been put order to protect the reaction wall from the specimen. The elastic foam is compressed so it exerts a force on the specimen that is possible to affect the results. In that test the compression is not significant so also the produced force is minor. However, when the velocity of the impacting mass will be increased (in the next tests) the deformation of the specimen will be bigger and in that case the produced force from the compression of the elastic foam might not be negligible. Moreover, when the impact load will be able to cause bigger damage on the specimen it is clear that this part of the apparatus will act as an obstacle in the development of the phenomenon. It is better in the future tests to increase the span between the rear part of the specimen and the elastic foam layer that protects the reaction wall.

Figure 51 presents the plastic strains on the specimen after the impact. The concrete part of the column presents some cracks (red coloured elements on the figure) in the middle rear part as a part of the flexural damage. The three main cracks can be identified also in the specimen after the impact (in the experiment). Plastic deformation can be observed also in the longitudinal reinforcement. The peak pressure that the specimen has been loaded in that experiments (according to the simulation values) is 3.3 MPa and the impulse 4100 kPa*ms. These values correspond to a scale distance $Z=1.153$ or a standoff distance of 11.53m for a charge of 1000 kg TNT, according to the AIRB routine [10], [11], [12]. The next tables present the corresponding blast data for the two tests that took place in the laboratory for both numerical and experimental data. It is obvious that the blast data from the numerical results correspond to more severe explosions. This is due to the higher peak force calculated in the numerical simulations.

Table 11: Blast data for the experiments (from the numerical values)

Experiment	Peak pressure [MPa]	Impulse [kPa*ms]	Z [m/kg³]	Standoff
Blast 15	0.38	2482	1.15	11.5
Blast 16	3.3	4100	1.25	12.5

Table 12: Blast data for the experiments (from the experimental values)

Experiment	Peak pressure [MPa]	Impulse [kPa*ms]	Z [m/kg³]	Standoff
Blast 15	0.16	1610	3.39	33.9
Blast 16	1.03	2760	1.71	17.1

5 Conclusions

The objective of this work is to verify the experimental results from the blast actuator test, with numerical simulation data. After some preliminary tests, the experimental device of the blast actuator is ready to proceed with test on real structural components. The first set of tests is taking place on a reinforced concrete column and the main target is to calibrate the apparatus and to correct possible inaccuracies.

The developed numerical model of the blast actuator is focusing on the impact of the mass with the specimen. The basic objective of the numerical simulations of the current report is the exact representation of the behaviour of the impacting mass the moment of the collision with the specimen. Therefore, special attention has been paid in the simulation of the contact of the elastic foam layer (located in the interface of the impacting mass and the specimen) with reinforced concrete column. A new material model connected to the elastic foam has been developed for that purpose with very encouraging results.

Two experimental tests are studied in the present work where the velocity of the impacting mass is varying. In the first test, the mass is impacting the specimen with 6.2m/s while in the second with 12m/s. The first test is not producing any damage in the specimen while the second one is causing some cracks in the rear part of the column due to flexural damage. The measuring quantities in the laboratory are the displacement of the impacting mass and the specimen, and the forces on the plates of the impacting mass and on the support of the specimen. The displacements are measured with an optical device and with a differentiation of the data, the velocity can be obtained. The forces are measured with load cells and the objective is to verify the values with the numerical results.

The comparison of the numerical results with the experimental ones are in general in good accordance. The duration of the phenomenon is the same in both cases while the profile of the curves for the displacement and the velocity of the impacting mass is similar. The major difference between the numerical and the experimental results is the magnitude of the peak contact force between the impactor and the specimen. The value obtained from the numerical simulation is almost 3 times higher than the experimental one. This results into a different calculation of the corresponding blast data based on the peak pressure and the impact of the load on the specimen.

It is not validated if the numerical results are overestimating the force or if the load cell measurement underestimated the input force. From the numerical point of view the representation of the elastic foam material is an under development procedure with many uncertainties concerning the material law and the selection of the coefficients of the energy equation that describes it. Also, the input data from the laboratory for the stress-strain curve of the elastic foam material they need more elaboration in order to include higher strain values and to take into account fast transient phenomena. It should be noted that the current elastic foam material has been selected after several tests and it seems that its behaviour is realistic.

On the other hand the experimental data obtained from the load cells is not clear if they depict the actual values. The load cells that measure the impact forces are located between the aluminium plates and the massive steel mass of the impacting object. It is clear that the measured force is filtered from the aluminium plates a fact that may justify the difference between the experimental and the numerical results. Another concerning fact is that the input and the output impulse calculated from the load cell data is not the same. The impulse expresses the change in the momentum of the system and its value can be calculated from the mass and the change of the velocity of the impacting mass. Moreover, the output impact is not higher than the input something that is unexpected.

Some differences between the two cases are observed on the results of the specimen. This difference can be explained from the fact that the material properties that has been used for the specimen (steel and concrete) are based on typical values and not on the actual ones (missing data from the constructor). These differences can be smoothed in the future calculation after obtaining more accurate input on the material properties of the specimen.

Another remark on the experimental configuration is that the aluminium plates of the impacting mass are loaded in such a way that they are plastified and a residual deformation is occurred. The plastification is not significant but in a more severe impact the aluminium plate might be

deformed in such a way that they will not be able to transport the load in a plane form. It is recommended that the configuration of the plates will change or with a thicker plate (but that will add mass at the front part of the impacting mass) or by changing the way that the aluminium plates are mounted through the load cell to the main part of the impacting mass.

It is recommended in the next tests to add some accelerometers on the impacting mass in order to control if the force that will be calculated from this measurement is in accordance with the data from the load cells. In addition, the distance between the rear part of the specimen and the elastic foam layer that protects the reaction wall should be increased so to ensure that a possible contact will not modify the results.

6 References

- [1] G. Valsamos, M. Larcher, G. Solomos, A. Anthoine, "Numerical Simulation in Support of the Blast Actuator Development", JRC Technical Reports, EUR 26430 EN, JRC86464, 2013.
- [2] M. Peroni, G. Solomos, G. Magonette, B. Viaccoz, P. Pegon, "Blast Simulator Setup Requirements", JRC Technical Reports, EUR 26018 EN, JRC79971 , 2013
- [3] EUROPLEXUS User's Manual. 2014.
- [4] <http://www-epx.cea.fr/>
- [5] <http://www-cast3m.cea.fr>
- [6] <http://www.paraview.org/>
- [7] T. Belytschko, M.O. Neal, "Contact-Impact by the Pinball Algorithm with Penalty and Lagrangian Methods", Int. J. Num. Meth. Engng, pp. 547-572, Vol. 31, 1991
- [8] F. Casadei, "A General Impact-Contact Algorithm Based on Hierarchic Pinballs for the EUROPLEXUS Software System", JRC Technical Note I.03.176, December 2003.
- [9] M. Larcher, G. Valsamos, G. Solomos, "Numerical material modelling for the blast actuator", JRC Technical Reports, EUR 26407 EN, JRC86348, 2013.
- [10] Kingery, Charles , Bulmash, Gerald, "Airblast Parameters from TNT Spherical Air Burst", Defense Technical Information Center, Ballistic Research Laboratory, Aberdeen Proving Ground, Maryland, 1984.
- [11] M. Larcher "Pressure-Time Functions for the Description of Air Blast Waves", JRC Technical Note , JRC46829, 2008.
- [12] M. Larcher, "Simulation of the Effects of an Air Blast Wave", JRC Technical Note, JRC41337, 2007.
- [13] Inc. ABAQUS. *ABAQUS - Theory Manual, Version 6.11*, 2014.
- [14] S. Kolling, P.A. Du Bois, D.J. Benson, and W.W. Feng. A tabulated formulation of hyperelastic with rate effects and damage. *Computational Mechanics*, 40:885–899, 2007
- [15] M. Schrodt, G. Benderoth, A. Kühhorn, and G. Silber. Hyperelastic description of polymer soft foams at finite deformations. *Technische Mechanik*, 25(3-4):162–173, 2005.
- [16] B. Storåkers. On material representation and constitutive branching in finite compressible elasticity. *Journal of the Mechanics and Physics of Solids*, 34(2):125–145, 1986.
- [17] D. Guilbaud. Damage plastic model for concrete failure under impulsive loadings. *XIII International Conference on Computational Plasticity. COMPLAS XIII, 1-3 September 2015, Barcelona Spain*.

7 Appendix

7.1 Blast

BASim3.dgibi

```
opti echo 1;
opti dime 3 elem cub8;
opti sauv form 'BASim3.msh';
opti trac psc ftra 'BASim3_mesh.ps';
*
camD = 100.0;
oelz = 0 0 camD;
oel = camD camD camD;
oeln = camD (0 - camD) (0 - camD);
oelm = (0 - camD) (0 + camD) (0 - camD);
tol = 1.E-3;
*Elle = 0.01/3;
Elle = 0.01/2;
ElleC = 0.02;
nc1 = 5;
*nc1 = 5;
nc3 = 4;
*nc3 = 5;
tha = 0.01;
thb = 0.015;
thc = 0.08;
*Elle = 0.01;
R1 = 0.02625;
R2 = 0.013125;
R3 = 0.005;
RR1 = R1*(0.5*(2**(0.5)));
RR2 = R2*(0.5*(2**(0.5)));
*The Y (half)dim of the plate
LY = 0.145;
*The X (half)dim of the plate
LX = 0.125;
LY2 = 0.1;
D12 = LY;
D23 = LX - R1;
D34 = R1 - R2;
D45 = R2;
D56 = R2;
D67 = R1 - R2;
D78 = LY2 - R3 - R1;
D89 = 2*R3;
D910 = LY - LY2 - R3;
D101 = LX;
P1 = 0 0 0;
P2 = P1 PLUS (0 D12 0);
n12 = ENTI ((D12 + 0.0001) / (Elle));
c12 = P1 D n12 P2;
P3 = P2 PLUS (D23 0 0);
n23 = ENTI ((D23 + 0.0001) / (Elle));
c23 = P2 D n23 P3;
P4 = P3 PLUS (D34 0 0);
n34 = ENTI ((D34 + 0.0001) / (Elle));
c34 = P3 D n34 P4;
P5 = P4 PLUS (D45 0 0);
P5n = P5 PLUS (0 0 1);
n45 = ENTI ((D45 + 0.0001) / (Elle));
c45 = P4 D n45 P5;
P6 = P5 PLUS (0 (0 - D56) 0);
n56 = ENTI ((D56 + 0.0001) / (Elle));
c56 = P5 D n56 P6;
P7 = P6 PLUS (0 (0 - D67) 0);
n67 = ENTI ((D67 + 0.0001) / (Elle));
c67 = P6 D n67 P7;
**
PC1 = P5 PLUS ((0 - RR1) (0 - RR1) 0);
PC2 = P5 PLUS ((0 - RR2) (0 - RR2) 0);
list RR1;
list RR2;
cc1 = CER3 nc1 P3 PC1 P7;
cc2 = CER3 nc1 P4 PC2 P6;
**
P8 = P7 PLUS (0 (0 - D78) 0);
n78 = ENTI ((D78 + 0.0001) / (Elle));
```

```
c78 = P7 D n78 P8;
*
P9 = P8 PLUS (0 (0 - D89) 0);
n89 = ENTI ((D89 + 0.0001) / (Elle));
c89 = P8 D n89 P9;
**
PC3 = P8 PLUS ((0 - R3) (0 - R3) 0);
cc3 = CER3 nc3 P8 PC3 P9;
**
**
P10 = P9 PLUS (0 (0 - D910) 0);
n910 = ENTI ((D910 + 0.0001) / (Elle));
c910 = P9 D n910 P10;
n101 = ENTI ((D101 + 0.0001) / (Elle));
c101 = P10 D n101 P1;

*ca = c12 ET c23 ET cc1 ET c78 ET c89 ET c910
ET c101;
ca = c12 ET c23 ET cc1 ET c78 ET cc3 ET c910 ET
c101;
sa = SURF (ca) PLAN;
saL = SURF (cc3 ET c89) PLAN;
**
cb = cc1 ET c67 ET cc2 ET c34;
sb = SURF (cb) PLAN;
**
cc = c45 ET c56 ET cc2;
sc = SURF (cc) PLAN;
***
***
*Second step part
P3U = P3 PLUS (0 0 thb);
P4U = P4 PLUS (0 0 thb);
P5U = P5 PLUS (0 0 thb);
P6U = P6 PLUS (0 0 thb);
P7U = P7 PLUS (0 0 thb);
PC1U = PC1 PLUS (0 0 thb);
PC2U = PC2 PLUS (0 0 thb);
c34U = c34 PLUS (0 0 thb);
c67U = c67 PLUS (0 0 thb);
c45U = c45 PLUS (0 0 thb);
c56U = c56 PLUS (0 0 thb);
***
LY3 = 0.3;
LY4 = 0.425;
P12U = P5U PLUS (0 (0 - LY3) 0);
P11U = P12U PLUS (0 R1 0);
P14U = P12U PLUS (0 (0 - R1) 0);
n711U = ENTI (((LY3 - (2*R1)) + 0.0001) /
(ElleC));
list n711U;
c711U = P7U D n711U P11U;
***
D1416U = LY4 - LY3 - R1;
n1416U = ENTI ((D1416U + 0.0001) / (ElleC));
P16U = P14U PLUS (0 (0 - D1416U) 0);
c1416U = P14U D n1416U P16U;
***
LX2 = 0.04;
D1617U = LX2;
n1617U = ENTI ((D1617U + 0.0001) / (ElleC));
P17U = P16U PLUS ((0 - D1617U) 0 0);
c1617U = P16U D n1617U P17U;
***
LX2 = 0.04;
D1718U = LY4;
n1718U = ENTI ((D1718U + 0.0001) / (ElleC));
P18U = P17U PLUS (0 D1718U 0);
c1718U = P17U D n1718U P18U;
***
D183U = LX2 - R1;
list D183U;
n183U = ENTI ((D183U + 0.0001) / (ElleC));
list n183U;
n183U = 1;
```

```

c183U = P18U D n183U P3U;
***
cc1U = cc1 PLUS (0 0 thb);
cc2U = cc2 PLUS (0 0 thb);
*
cc1UM = cc1U SYME PLAN P18U P5U P5;
TRAC oelz CACH QUAL ( cc1U ET cc1Um ET P18U ET
P5U ET P5);
TRAC oel CACH QUAL ( cc1U ET cc1Um ET P18U ET
P5U ET P5);

cc2UM = cc2U SYME PLAN P18U P5U P5;
cc1NU = cc1U ET cc1UM;
cc2NU = cc2U ET cc2UM;
*
cc4U = cc1NU PLUS (0 (0 - LY3) 0);
cc5U = cc2NU PLUS (0 (0 - LY3) 0);
***
cU = c711U ET c1416U ET c1617U ET c1718U ET
c183U;
cU = cU ET cc1U ET cc2U ET cc4U ET cc5U;
**TRAC oel CACH QUAL (cU);
***

elim tol (c1718U ET c183U ET cc1U ET c711U ET
cc4U
ET c1416U ET c1617U);
**TRAC oel CACH QUAL (c1718U ET c183U ET cc1U
ET c711U ET cc4U
**ET c1416U ET c1617U);
cau = c1718U ET c183U ET cc1U ET c711U ET cc4U
ET c1416U ET c1617U;
sau = SURF (cau) PLAN;
**
elim tol (cc1U ET c67U ET cc2U ET c34U);
cbu = cc1U ET c67U ET cc2U ET c34U;
sbu = SURF (cbu) PLAN;
**
elim tol (c45U ET c56U ET cc2U);
ccu = c45U ET c56U ET cc2U;
scu = SURF (ccu) PLAN;
**
sbum = sbu SYME PLAN P18U P5U P5;
scum = scu SYME PLAN P18U P5U P5;
sdu = (sbum ET sbu ET scum ET scu) PLUS (0 (0 -
LY3) 0);
*
elim tol (sau ET sbu ET scu ET sdu);
**TRAC oel CACH QUAL (sau ET sbu ET scu ET
sdu);
nthc = ENTI ((thc + 0.0001) / (ElleC));
vc = (sau ET sbu ET scu ET sdu) VOLU TRAN nthc
(0 0 thc);
vcml = vc SYME PLAN P10 P5 P5n;
vcml2 = (vc ET vcml) SYME PLAN P2 P5 P5n;
meshMass = vc ET vcml ET vcml2;
TRAC oel CACH QUAL (vc);
TRAC oel CACH QUAL (vcml);
TRAC oel CACH QUAL (vcml2);
***
ntha = ENTI (((1*tha) + 0.0001) / (Elle));
TRAC oel CACH QUAL (sa);
TRAC oel CACH QUAL (sb);
TRAC oel CACH QUAL (sc);
va = (sa ET sb ET sc) VOLU TRAN ntha (0 0 (0 -
(1*tha)));
sf = (sa ET sb ET sc ET saL) PLUS (0 0 (0 -
(1*tha)));
snfo = 6;
nfo = ENTI (((snfo*tha) + 0.0001) / (Elle));
vf = sf VOLU TRAN nfo (0 0 (0 - (snfo*tha)));
nthb = ENTI ((thb + 0.0001) / (Elle));
vb = (sb) VOLU TRAN nthb (0 0 (0 + thb));
TRAC oel CACH QUAL (va);
TRAC oel CACH QUAL (vb);
TRAC oel CACH QUAL (vf);
meshA = va ET vb ET vf;
meshB = meshA SYME PLAN P10 P5 P5n;
meshC = (meshA ET meshB) SYME PLAN P2 P5 P5n;
meshP = meshA ET meshB ET meshC;

meshP2 = meshP PLUS (0 LY3 0);
meshP3 = meshP PLUS (0 (0 - LY3) 0);
*
Zsp = (snfo + 1)*tha + (ElleC/2) + 0.005;
Hcol = 2.2;
Ycl = Hcol/2.0;
Wcl = 0.25;
Xcl = Wcl/2.0;
Dcl = 0.25;
Pcol1 = (0 - (Xcl - D101)) (0 - (Ycl - D12)) (0
- Zsp);
Pcol2 = Pcol1 PLUS (0 Hcol 0);
ElleCC = 1*ElleC;
ncy = ENTI ((Hcol + 0.0001) / (ElleCC));
cc1 = Pcol1 D ncy Pcol2;
ncx = ENTI ((Wcl + 0.0001) / (ElleCC));
list ncx;
sc1 = cc1 TRAN ncx (Wcl 0 0);
ncz = ENTI ((Dcl + 0.0001) / (ElleCC));
vc1 = (sc1) VOLU TRAN ncz (0 0 (0 - Dcl));
Dri = 0.035;
Pri1 = Pcol1 PLUS ((0 + Dri) 0 (0 - Dri));
Pri2 = Pri1 PLUS (0 Hcol 0);
cri1 = Pri1 D ncy Pri2;
ritr = Wcl - (2*Dri);
cri2 = cri1 PLUS ((ritr) 0 0);
cri3 = cri2 PLUS (0 0 (0 - ritr));
cri4 = cri1 PLUS (0 0 (0 - ritr));
barsV = cri1 ET cri2 ET cri3 ET cri4;
DriS = 0.015;
HriS = 0.2;
PriS1 = Pcol1 PLUS ((0 + DriS) HriS (0 -
DriS));
ritrS = Wcl - (2*DriS);
PriS2 = PriS1 PLUS ((ritrS) 0 0);
PriS3 = PriS2 PLUS (0 0 (0 - ritrS));
PriS4 = PriS1 PLUS (0 0 (0 - ritrS));
nriS = ENTI ((ritrS + 0.0001) / (ElleCC));
criSa = PriS1 D nriS PriS2;
criSb = PriS2 D nriS PriS3;
criSc = PriS3 D nriS PriS4;
criSd = PriS4 D nriS PriS1;
barS1 = criSa ET criSb ET criSc ET criSd;
barS2 = barS1 PLUS (0 Hris 0);
barS3 = barS2 PLUS (0 Hris 0);
barS4 = barS3 PLUS (0 Hris 0);
barS5 = barS4 PLUS (0 Hris 0);
barS6 = barS5 PLUS (0 Hris 0);
barS7 = barS6 PLUS (0 Hris 0);
barS8 = barS7 PLUS (0 Hris 0);
barS9 = barS8 PLUS (0 Hris 0);
barS10 = barS9 PLUS (0 Hris 0);
barsS = barS1 ET barS2 ET barS3 ET barS4 ET
barS5
ET barS6 ET barS7 ET barS8 ET barS9 ET barS10;
*
bars = barsV ET barsS;
TRAC oel cach qual (bars);
TRAC oel cach qual (vc1 ET cri1);
*
mesh = meshP ET meshP2 ET meshP3 ET meshMass ET
vc1 ET bars;
TRAC oel CACH QUAL (mesh);
TRAC oeln CACH QUAL (mesh);
mesh = mesh coul jaun;
elim tol mesh;
penta = mesh ELEM 'PRI6';
hexa = mesh ELEM 'CUB8';
TASS mesh NOOP;
SAUV FORM mesh;
LIST (NBEL mesh);
LIST (NBEL penta);
LIST (NBEL hexa);
LIST (NBNO mesh);
LIST (NBNO (sa ET sb Et sc));

*TRAC qual cach (ca);
*TRAC qual cach (sa);
*TRAC oelz CACH QUAL (ca);
*TRAC oelz CACH QUAL (sa);

```

```

*TRAC oelz CACH QUAL (cb);
*TRAC oelz CACH QUAL (sb);
*TRAC oelz CACH QUAL (sc);
TRAC oelz CACH QUAL (sa ET sb Et sc);
TRAC oel CACH QUAL (mesh);
*
Fin;

```

Blast15.epx

```

PLATE
ECHO
CONV WIN
*CAST 'BASim3.msh' mesh
CAST mesh
TRID LAGR 'EROS 0.0
DIME
* DEBR 30720
TERM
GEOM cube hexa pris penta BR3D bars TERM
*GEOM cub8 hexa pr6 penta TERM
COMP
* EPAI 3.1416E-4 LECT bars TERM
  SECT 1.131E-4 LECT barsV TERM
  SECT 0.50265E-4 LECT barsS TERM
  GROU 12 'MES' LECT mesh TERM
    COND ZB GT 0.0
    COND ZB LT 0.014999
  'MAS' LECT mesh TERM
    COND ZB GT 0.015
  'FOA' LECT mesh TERM
    COND ZB LT -0.0099
    COND ZB GT -0.0699
  'WAL' LECT mesh TERM
    COND ZB LT -0.07499
  'WALC' LECT mesh TERM
    COND ZB LT -0.07499
    COND ZB GT -0.0955
    COND YB GT -0.34
    COND YB LT 0.62
  'PLA' LECT mesh TERM
    COND ZB LT 0.0
    COND ZB GT -0.01001
  'PLA1' LECT mesh TERM
    COND ZB LT 0.0
    COND ZB GT -0.01001
    COND YB LT -0.001
  'PLA2' LECT mesh TERM
    COND ZB LT 0.0
    COND ZB GT -0.01001
    COND YB GT -0.001
    COND YB LT 0.29001
  'PLA3' LECT mesh TERM
    COND ZB LT 0.0
    COND ZB GT -0.01001
    COND YB GT 0.28999
  'MES1' LECT mesh TERM
    COND ZB GT 0.0
    COND ZB LT 0.014999
    COND YB GT 0.0
    COND YB LT 0.2
  'MES2' LECT mesh TERM
    COND ZB GT 0.0
    COND ZB LT 0.014999
    COND YB GT 0.23
  'MES3' LECT mesh TERM
    COND ZB GT 0.0
    COND ZB LT 0.014999
    COND YB LT -0.1
COUL GR30 LECT WAL TERM
GR80 LECT MESH diff WAL FOA TERM
TURQ LECT FOA TERM
NGRO 4 'fix1' LECT WAL TERM COND Z LT -0.329
  COND Y GT 1.135
  COND Y LT 1.145
  'fix2' LECT WAL TERM COND Z LT -0.329
    COND Y LT -0.835
    COND Y GT -0.855

```

```

'coIF' LECT WAL TERM COND NEAR POIN 0.125 0.145 -
0.07
'coIR' LECT WAL TERM COND NEAR POIN 0.125 0.145 -
0.335
MATE
  VMIS ISOT
    RO 7800 YOUN 200E9 NU 0.3 ELAS 850.E6
    FAIL 2 LIM1 0.12
    TRAC 2 850.0E6 0.00425
      1035.2E6 0.12
    LECT bars term
  VMIS PARF !ALU
    RO 2800 YOUN 70E9 NU 0.35 ELAS 400E6
    LECT mesh diff MES WAL FOA MAS bars term
  VM23 RO 7444.0 YOUN 2.1E11 NU 0.3
    ELAS 400.0E6
    TRAC 1 400.E6 0.0019
    LECT MAS TERM
  VM23 RO 6488.108 YOUN 1.317E11 NU 0.3
    ELAS 400.0E6
    TRAC 1 400.E6 0.00305
    LECT MES TERM
  DPDC RO 2400 YOUN 30E+9 NU 0.21
    FC 20.E+6 DAGG 20.0E-3 VERS 7 EFVI
    LECT WAL TERM
  HYPE TYPE 5
  RO 42.0
  CO1 0.72865E+02
  CO2 0.72297E+02
  CO5 0.20123E+05
  CO6 0.90712E+02
  CO9 0.16805E-01
  CO10 0.64908E-01
  LECT FOA TERM
LINK COUP
  BLOQ 3 LECT fix1 fix2 TERM
  Armat beton lecture wal TERM
  ferr lecture bars term
  PINB BODY LECT FOA TERM
  BODY LECT WALC TERM
INIT VITE 3 -6.1 LECT mesh diff WAL bars TERM
REGI 'WAL' TOUT LECT WAL TERM
  'MAS' TOUT LECT MAS TERM
  'PLA' TOUT LECT PLA TERM
  'FOA' TOUT LECT FOA TERM
  'MES' TOUT LECT MES TERM
  'BAR' TOUT LECT BARS TERM
  'fix1' TOUT POIN LECT fix1 TERM
  'fix2' TOUT POIN LECT fix2 TERM
  'walc' TOUT POIN LECT walc TERM
  'MES1' TOUT LECT MES1 TERM
  'MES2' TOUT LECT MES2 TERM
  'MES3' TOUT LECT MES3 TERM
ECRI DEPL TFRE 5.E-5
  POINT LECT 1 TERM
  ELEM LECT 1 TERM
  FICH SPLI ALIC TFRE 5.E-5
* Fichier Format PVTK TFREQ 5.e-5
* GROU 6 OBJET WAL TERM
* OBJET PLA TERM
* OBJET FOA TERM
* OBJET MES TERM
* OBJET MAS TERM
* OBJET bars TERM
* vari depl ecrou vite cont FLIA
OPTI NOTE
  CSTA 0.8
  LOG 1
  JAUM
  PINS GRID DGRI
! REND SAFE
CALC TINI 0 TEND 30.E-3 TFAI 1.5e-8
SUIT
BASIM3B
ECHO
RESU SPLI ALIC GARD PSCR
SORT GRAP
AXTE 1.0 'Time [s]'
*MAS

```

COUR 1 'VelAvMAS' VMOY COMP 3 REGI 2
 TRAC 1 AXES 1.0 'velAvMAS. [m/s]' YZER
 LIST 1 AXES 1.0 'Velocity' YZER
 COUR 2 'AccAvMAS' DIFF 1
 TRAC 2 AXES 1.0 'AccAvMAS. [m/s^2]' YZER
 LIST 2 AXES 1.0 'Acceleration' YZER
 COUR 3 'DisAvMAS' INT 1
 TRAC 3 AXES 1.0 'DisAvMAS. [m]' YZER
 LIST 3 AXES 1.0 'Displacement' YZER
 *MES
 COUR 11 'VelAvMES' VMOY COMP 3 REGI 5
 TRAC 11 AXES 1.0 'velAvMES. [m/s]' YZER
 COUR 12 'AccAvMES' DIFF 11
 TRAC 12 AXES 1.0 'AccAvMES. [m/s^2]' YZER
 COUR 13 'DisAvMES' INT 11
 TRAC 13 AXES 1.0 'DisAvMES. [m]' YZER
 *PLA
 COUR 21 'VelAvPLA' VMOY COMP 3 REGI 3
 TRAC 21 AXES 1.0 'velAvPLA. [m/s]' YZER
 COUR 22 'AccAvPLA' DIFF 21
 TRAC 22 AXES 1.0 'AccAvPLA. [m/s^2]' YZER
 COUR 23 'DisAvPLA' INT 21
 TRAC 13 AXES 1.0 'DisAvMES. [m]' YZER
 *Contact Column
 COUR 31 'ConFCol' FLIR COMP 3 REGI 9
 TRAC 31 AXES 1.0 'ConFCol. [N]' YZER
 COUR 32 'ConPCol' MULC 31 4.5977
 TRAC 32 AXES 1.0 'ConPCol. [Pa]' YZER
 COUR 33 'ImpCol' INT 32
 TRAC 33 AXES 1.0 'ImpCol. [Pa*s]' YZER
 COUR 34 'ImpCol' INT 31
 TRAC 34 AXES 1.0 'ImpColF. [N*s]' YZER
 *Contact FOA
 COUR 41 'ConFCol' FLIR COMP 3 REGI 4
 TRAC 41 AXES 1.0 'ConFFoa. [N]' YZER
 LIST 41 AXES 1.0 'ConFor' YZER
 COUR 42 'ConPFoa' MULC 41 4.5977
 TRAC 42 AXES 1.0 'ConPFoa. [Pa]' YZER
 LIST 42 AXES 1.0 'ConPres' YZER
 COUR 43 'ImpFoa' INT 42
 TRAC 43 AXES 1.0 'ImpFoa. [Pa*s]' YZER
 LIST 43 AXES 1.0 'ConImp' YZER
 COUR 44 'ImpCol' INT 41
 TRAC 44 AXES 1.0 'ImpFoaF. [N*s]' YZER
 LIST 44 AXES 1.0 'ConImpF' YZER
 *FIX forces
 COUR 51 'FixF1' RESU COMP 3 REGI 7
 TRAC 51 AXES 1.0 'FixF1. [N]' YZER
 LIST 51 AXES 1.0 'FixF1' YZER
 COUR 52 'FixF2' RESU COMP 3 REGI 8
 TRAC 52 AXES 1.0 'FixF2. [N]' YZER
 LIST 52 AXES 1.0 'FixF2' YZER
 COUR 53 'ImpFix1' INT 51
 TRAC 53 AXES 1.0 'ImpFix1. [N*s]' YZER
 COUR 54 'ImpFix2' INT 52
 TRAC 54 AXES 1.0 'ImpFix2. [N*s]' YZER
 COUR 55 'ImpFixT' SOMME 2 53 1.0 54 1.0
 TRAC 55 AXES 1.0 'ImpFixT. [N*s]' YZER
 LIST 55 AXES 1.0 'FixImpFTot' YZER
 *
 COUR 91 'DisColF' DEPL COMP 3 POIN LECT colF TERM
 TRAC 91 AXES 1.0 'DisColF' YZER
 LIST 91 AXES 1.0 'DisColF' YZER
 COUR 92 'DisColR' DEPL COMP 3 POIN LECT colR TERM
 TRAC 92 AXES 1.0 'DisColR' YZER
 LIST 92 AXES 1.0 'DisColR' YZER
 COUR 93 'DeflCol' SUB 92 91
 TRAC 93 AXES 1.0 'DifCol' YZER
 *
 COUR 101 'VelColF' VITE COMP 3 POIN LECT colF TERM
 TRAC 101 AXES 1.0 'VelColF' YZER
 LIST 101 AXES 1.0 'VelColF' YZER
 COUR 102 'VelColR' VITE COMP 3 POIN LECT colR TERM
 TRAC 102 AXES 1.0 'VelColR' YZER
 *ECRO1 FOA
 COUR 111 'Ecro1Foa' ECRM COMP 1 REGI 4
 TRAC 111 AXES 1.0 'Ecro1Foa. [Pa]' YZER
 COUR 112 'Ecro2Foa' ECRM COMP 2 REGI 4
 TRAC 112 AXES 1.0 'Ecro2Foa. [Pa]' YZER

LIST 112 AXES 1.0 'StressFoa' YZER
 COUR 113 'Ecro3Foa' ECRM COMP 3 REGI 4
 TRAC 113 AXES 1.0 'Ecro3Foa. [-]' YZER

 FIN

Blast16.epx

PLATE
 ECHO
 CONV WIN
 *CAST 'BASim3.msh' mesh
 CAST mesh
 TRID LAGR !EROS 0.0
 DIME
 * DEBR 30720
 TERM
 GEOM cube hexa pris penta BR3D bars TERM
 *GEOM cub8 hexa pr6 penta TERM
 COMP
 * EPAI 3.1416E-4 LECT bars TERM
 SECT 1.131E-4 LECT barsV TERM
 SECT 0.50265E-4 LECT barsS TERM
 GROU 12 'MES' LECT mesh TERM
 COND ZB GT 0.0
 COND ZB LT 0.014999
 'MAS' LECT mesh TERM
 COND ZB GT 0.015
 'FOA' LECT mesh TERM
 COND ZB LT -0.0099
 COND ZB GT -0.0699
 'WAL' LECT mesh TERM
 COND ZB LT -0.07499
 'WALC' LECT mesh TERM
 COND ZB LT -0.07499
 COND ZB GT -0.0955
 COND YB GT -0.34
 COND YB LT 0.62
 'PLA' LECT mesh TERM
 COND ZB LT 0.0
 PLA1' LECT mesh TERM
 COND ZB LT 0.0
 COND ZB GT -0.01001
 COND YB LT -0.001
 PLA2' LECT mesh TERM
 COND ZB LT 0.0
 COND ZB GT -0.01001
 COND YB GT -0.001
 COND YB LT 0.29001
 PLA3' LECT mesh TERM
 COND ZB LT 0.0
 COND ZB GT -0.01001
 COND YB GT 0.28999
 'MES1' LECT mesh TERM
 COND ZB GT 0.0
 COND ZB LT 0.014999
 COND YB GT 0.0
 COND YB LT 0.2
 'MES2' LECT mesh TERM
 COND ZB GT 0.0
 COND ZB LT 0.014999
 COND YB GT 0.23
 'MES3' LECT mesh TERM
 COND ZB GT 0.0
 COND ZB LT 0.014999
 COND YB LT -0.1
 COUL GR30 LECT WAL TERM
 GR80 LECT MESH diff WAL FOA TERM
 TURQ LECT FOA TERM
 NGRO 4 'fix1' LECT WAL TERM COND Z LT -0.329
 COND Y GT 1.135
 COND Y LT 1.145
 'fix2' LECT WAL TERM COND Z LT -0.329
 COND Y LT -0.835
 COND Y GT -0.855
 'colF' LECT WAL TERM COND NEAR POIN 0.125 0.145 -

0.07

'colR' LECT WAL TERM COND NEAR POIN 0.125 0.145 -
0.335
MATE
VMIS ISOT
RO 7800 YOUN 200E9 NU 0.3 ELAS 850.E6
FAIL 2 LIM1 0.12
TRAC 2 850.0E6 0.00425
1035.2E6 0.12
LECT bars term
VMIS PARF !ALU
RO 2800 YOUN 70E9 NU 0.35 ELAS 400E6
LECT mesh diff MES WAL FOA MAS bars term
VM23 RO 7444.0 YOUN 2.1E11 NU 0.3
ELAS 400.0E6
TRAC 1 400.E6 0.0019
LECT MAS TERM
VM23 RO 6488.108 YOUN 1.317E11 NU 0.3
ELAS 400.0E6
TRAC 1 400.E6 0.00305
LECT MES TERM
DPDC RO 2400 YOUN 30E+9 NU 0.21
FC 20.E+6 DAGG 20.0E-3 VERS 7 EFV1
LECT WAL TERM
HYPE TYPE 5
RO 42.0
CO1 0.72865E+02
CO2 0.72297E+02
CO5 0.20123E+05
CO6 0.90712E+02
CO9 0.16805E-01
CO10 0.64908E-01
LECT FOA TERM
LINK COUP
BLOQ 3 LECT fix1 fix2 TERM
Armat beton lecture wal TERM
ferr lecture bars term
PINB BODY LECT FOA TERM
BODY LECT WALC TERM
INIT VITE 3 -12.0 LECT mesh diff WAL bars TERM
REGI 'WAL' TOUT LECT WAL TERM
'MAS' TOUT LECT MAS TERM
'PLA' TOUT LECT PLA TERM
'FOA' TOUT LECT FOA TERM
'MES' TOUT LECT MES TERM
'BAR' TOUT LECT BARS TERM
'fix1' TOUT POIN LECT fix1 TERM
'fix2' TOUT POIN LECT fix2 TERM
'walc' TOUT POIN LECT walc TERM
'MES1' TOUT LECT MES1 TERM
'MES2' TOUT LECT MES2 TERM
'MES3' TOUT LECT MES3 TERM
ECRI DEPL TFRE 5.E-5
POINT LECT 1 TERM
ELEM LECT 1 TERM
FICH SPLI ALIC TFRE 5.E-5
* Fichier Format PVTK TFREQ 5.e-5
* GROU 6 OBJET WAL TERM
* OBJET PLA TERM
* OBJET FOA TERM
* OBJET MES TERM
* OBJET MAS TERM
* OBJET bars TERM
* vari depl ecrou vite cont FLIA
OPTI NOTE
CSTA 0.8
LOG 1
JAUM
PINS GRID DGRI
! REND SAFE
CALC TINI 0 TEND 30.E-3 TFAI 1.5e-8
SUIT
BASIM3B
ECHO
RESU SPLI ALIC GARD PSCR
SORT GRAP
AXTE 1.0 'Time [s]'
*MAS
COUR 1 'VelAvMAS' VMOY COMP 3 REGI 2
TRAC 1 AXES 1.0 'velAvMAS. [m/s]' YZER

LIST 1 AXES 1.0 'Velocity' YZER
COUR 2 'AccAvMAS' DIFF 1
TRAC 2 AXES 1.0 'AccAvMAS. [m/s^2]' YZER
LIST 2 AXES 1.0 'Acceleration' YZER
COUR 3 'DisAvMAS' INT 1
TRAC 3 AXES 1.0 'DisAvMAS. [m]' YZER
LIST 3 AXES 1.0 'Displacement' YZER
*MES
COUR 11 'VelAvMES' VMOY COMP 3 REGI 5
TRAC 11 AXES 1.0 'velAvMES. [m/s]' YZER
COUR 12 'AccAvMES' DIFF 11
TRAC 12 AXES 1.0 'AccAvMES. [m/s^2]' YZER
COUR 13 'DisAvMES' INT 11
TRAC 13 AXES 1.0 'DisAvMES. [m]' YZER
*PLA
COUR 21 'VelAvPLA' VMOY COMP 3 REGI 3
TRAC 21 AXES 1.0 'velAvPLA. [m/s]' YZER
COUR 22 'AccAvPLA' DIFF 21
TRAC 22 AXES 1.0 'AccAvPLA. [m/s^2]' YZER
COUR 23 'DisAvPLA' INT 21
TRAC 13 AXES 1.0 'DisAvMES. [m]' YZER
*Contact Column
COUR 31 'ConFCol' FLIR COMP 3 REGI 9
TRAC 31 AXES 1.0 'ConFCol. [N]' YZER
COUR 32 'ConPCol' MULC 31 4.5977
TRAC 32 AXES 1.0 'ConPCol. [Pa]' YZER
COUR 33 'ImpCol' INT 32
TRAC 33 AXES 1.0 'ImpCol. [Pa*s]' YZER
COUR 34 'ImpCol' INT 31
TRAC 34 AXES 1.0 'ImpColF. [N*s]' YZER
*Contact FOA
COUR 41 'ConFCol' FLIR COMP 3 REGI 4
TRAC 41 AXES 1.0 'ConFFoa. [N]' YZER
LIST 41 AXES 1.0 'ConFor' YZER
COUR 42 'ConPFoa' MULC 41 4.5977
TRAC 42 AXES 1.0 'ConPFoa. [Pa]' YZER
LIST 42 AXES 1.0 'ConPres' YZER
COUR 43 'ImpFoa' INT 42
TRAC 43 AXES 1.0 'ImpFoa. [Pa*s]' YZER
LIST 43 AXES 1.0 'ConImp' YZER
COUR 44 'ImpCol' INT 41
TRAC 44 AXES 1.0 'ImpFoaF. [N*s]' YZER
LIST 44 AXES 1.0 'ConImpF' YZER
*FIX forces
COUR 51 'FixF1' RESU COMP 3 REGI 7
TRAC 51 AXES 1.0 'FixF1. [N]' YZER
LIST 51 AXES 1.0 'FixF1' YZER
COUR 52 'FixF2' RESU COMP 3 REGI 8
TRAC 52 AXES 1.0 'FixF2. [N]' YZER
LIST 52 AXES 1.0 'FixF2' YZER
COUR 53 'ImpFix1' INT 51
TRAC 53 AXES 1.0 'ImpFix1. [N*s]' YZER
COUR 54 'ImpFix2' INT 52
TRAC 54 AXES 1.0 'ImpFix2. [N*s]' YZER
COUR 55 'ImpFixT' SOMME 2 53 1.0 54 1.0
TRAC 55 AXES 1.0 'ImpFixT. [N*s]' YZER
LIST 55 AXES 1.0 'FixImpFTot' YZER
*
COUR 91 'DisColF' DEPL COMP 3 POIN LECT colF TERM
TRAC 91 AXES 1.0 'DisColF' YZER
LIST 91 AXES 1.0 'DisColF' YZER
COUR 92 'DisColR' DEPL COMP 3 POIN LECT colR TERM
TRAC 92 AXES 1.0 'DisColR' YZER
LIST 92 AXES 1.0 'DisColR' YZER
COUR 93 'DeflCol' SUB 92 91
TRAC 93 AXES 1.0 'DifCol' YZER
*
COUR 101 'VelColF' VITE COMP 3 POIN LECT colF TERM
TRAC 101 AXES 1.0 'VelColF' YZER
LIST 101 AXES 1.0 'VelColF' YZER
COUR 102 'VelColR' VITE COMP 3 POIN LECT colR TERM
TRAC 102 AXES 1.0 'VelColR' YZER
*ECRO1 FOA
COUR 111 'Ecro1Foa' ECRM COMP 1 REGI 4
TRAC 111 AXES 1.0 'Ecro1Foa. [Pa]' YZER
COUR 112 'Ecro2Foa' ECRM COMP 2 REGI 4
TRAC 112 AXES 1.0 'Ecro2Foa. [Pa]' YZER
LIST 112 AXES 1.0 'StressFoa' YZER
COUR 113 'Ecro3Foa' ECRM COMP 3 REGI 4

TRAC 113 AXES 1.0 'Ecro3Foa. [-]' YZER

FIN

Europe Direct is a service to help you find answers to your questions about the European Union
Free phone number (*): 00 800 6 7 8 9 10 11
(*) Certain mobile telephone operators do not allow access to 00 800 numbers or these calls may be billed.

A great deal of additional information on the European Union is available on the Internet.
It can be accessed through the Europa server <http://europa.eu>

How to obtain EU publications

Our publications are available from EU Bookshop (<http://bookshop.europa.eu>),
where you can place an order with the sales agent of your choice.

The Publications Office has a worldwide network of sales agents.
You can obtain their contact details by sending a fax to (352) 29 29-42758.

JRC Mission

As the Commission's in-house science service, the Joint Research Centre's mission is to provide EU policies with independent, evidence-based scientific and technical support throughout the whole policy cycle.

Working in close cooperation with policy Directorates-General, the JRC addresses key societal challenges while stimulating innovation through developing new methods, tools and standards, and sharing its know-how with the Member States, the scientific community and international partners.

*Serving society
Stimulating innovation
Supporting legislation*

